

1163-86281

Technical Report No. 32-68

**Interplanetary Trajectories and Payload
Capabilities of Advanced
Propulsion Vehicles**

W. G. Melbourne



**JET PROPULSION LABORATORY
CALIFORNIA INSTITUTE OF TECHNOLOGY
PASADENA, CALIFORNIA**

March 31, 1961

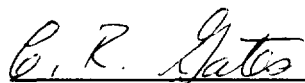
Sgt 32638

NATIONAL AERONAUTICS AND SPACE ADMINISTRATION
CONTRACT NO. NASW-6

Technical Report No. 32-68

**INTERPLANETARY TRAJECTORIES AND PAYLOAD
CAPABILITIES OF ADVANCED PROPULSION VEHICLES**

W. G. Melbourne

A handwritten signature in cursive script, reading "C. R. Gates", is positioned above a horizontal line.

C. R. Gates, *Chief*
Systems Analysis Section

JET PROPULSION LABORATORY
CALIFORNIA INSTITUTE OF TECHNOLOGY
PASADENA, CALIFORNIA
March 31, 1961

Copyright © 1961
Jet Propulsion Laboratory
California Institute of Technology

CONTENTS

I.	Introduction	1
II.	Fundamentals of Power-Limited Propulsion Systems	2
A.	Rocket Equation for Power-Limited Flight	4
B.	Allocation of M_L , M_W , and M_P	4
C.	The Minimization of β	6
III.	Interplanetary Vehicle Performance Characteristics	10
IV.	Planetocentric Spiral Trajectories	15
V.	Numerical Example of Vehicle Payload Capabilities	20
	References	23
	Tables	24
	Figures	43
Appendixes		
A.	Analytical Basis of Thrust Program	60
B.	Origin and Utilization of Expressions Describing Planetocentric Portions of Interplanetary Trajectories	63

TABLES

1.	Specific impulse and thrust acceleration of several propulsion systems	24
2.	Mercury orbiter trajectories	25
3.	Venus orbiter trajectories	28
4.	Mars orbiter trajectories	29
5.	Jupiter orbiter trajectories	33
6.	Saturn orbiter trajectories	34
7.	Mercury flyby trajectories (apogee encounter)	35

TABLES (Cont'd)

8.	Venus flyby trajectories	36
9.	Mars flyby trajectories (mean distance encounter)	37
10.	Jupiter flyby trajectories (mean distance encounter)	38
11.	Saturn flyby trajectories (mean distance encounter)	39
12.	Three-dimensional optimum thrust trajectories	40
13.	Equatorial radii and orbital velocities of orbits of various altitudes	41
14.	Weight percentage comparison for chemical and advanced systems	42

FIGURES

1.	Payload on structures mass ratio vs powerplant mass ratio	43
2.	Payload on structures mass ratio vs powerplant mass ratio	43
3.	Payload capabilities: Mercury trajectories	44
4.	Payload capabilities: Mercury orbiter trajectories	45
5.	Payload capabilities: Venus trajectories	46
6.	Payload capabilities: Mars trajectories	47
7.	Payload capabilities: Mars orbiter trajectories	48
8.	Payload capabilities: Jupiter trajectories	49
9.	Payload capabilities: Saturn trajectories	50
10.	Mercury orbiter trajectories	51
11.	Mars orbiter trajectories	51
12.	Power-limited optimum thrust program: initial thrust acceleration	52
13.	Power-limited optimum thrust program: initial thrust angle	52
14.	Power-limited optimum thrust program: initial time derivative of the radial thrust acceleration	53

FIGURES (Cont'd)

15.	Power-limited optimum thrust program	53
16.	Mars orbiting trajectories, 30-day heliocentric flight time, two-dimensional optimum thrust program for power-limited propulsion	54
17.	Mars orbiting trajectories, 178-day heliocentric flight time, three-dimensional optimum thrust program for power-limited propulsion	54
18.	Mars orbiting trajectories, 178-day heliocentric flight time, three-dimensional optimum thrust program for power-limited propulsion	55
19.	Mars orbiting trajectories, 178-day heliocentric flight time, three-dimensional optimum thrust program for power-limited propulsion	55
20.	Venus orbiting trajectories, 120-day heliocentric flight time, three-dimensional optimum thrust program for power-limited propulsion	56
21.	Venus orbiting trajectories, 120-day heliocentric flight time, three-dimensional optimum thrust program for power-limited propulsion	56
22.	Venus orbiting trajectories, 120-day heliocentric flight time, three-dimensional optimum thrust program for power-limited propulsion	57
23.	Jupiter trajectories, 510-day heliocentric flight time, two-dimensional optimum thrust program for power-limited propulsion	57
24.	Earth-centered low thrust trajectory	58
25.	Correction factor for constant tangential thrust	59
26.	Variation of escape time with vehicle mass loss	59

ABSTRACT

This paper presents a résumé of current studies of the systematics of low-thrust interplanetary trajectories employing, generally, an optimized thrust program for power-limited flight. Primarily, the analysis is two-dimensional, although several three-dimensional examples are presented showing the effects of non-coplanar orbit transfer. Accompanying each trajectory is its value of $\int_0^T a^2 dt$. This quantity is analogous to the concept of characteristic velocity of chemical rockets and is an index of the vehicle performance (e.g., propellant requirement) for the particular mission. Trajectories are presented for the following mission types: (1) the orbiter or rendezvous mission, and (2) the flyby mission. The former type possesses terminal conditions identical with the heliocentric kinematic conditions of the target planet; the latter type encounters the target planet with no directly specified velocity conditions. Both types of trajectories have been computed for the following planets and ranges of heliocentric flight time:

Mercury	30 - 360 days
Venus	30 - 360
Mars	30 - 420
Jupiter	180 - 900
Saturn	180 - 900

For Mercury and Mars missions, both circular and the appropriate eccentric orbits were adopted. Circular orbits were assumed for the other planets, including Earth.

A review of the basic concepts appropriate for power-limited vehicles is presented. Approximate methods for describing the geocentric and planetocentric spiral portions of the transfer trajectories are presented as well as methods for obtaining vehicle performances in these regions. A sample comparison with digital results is presented.

The work completed is of a preliminary nature and serves as a basis for further studies whose ultimate aim is to define a standard trajectory for a specified mission and a thrust program which yields a near optimum payload and is compatible with the engineering constraints arising from the vehicle and propulsion system design. The thrust program employed in these studies in some cases does not satisfy these engineering constraints. On the other hand, the results presented here yield upper bounds on payload capabilities for each mission considered. Subsequent studies will utilize alternate thrust programs of a near optimum nature but more generally compatible with engineering constraints.

I. INTRODUCTION

The primary purpose of this paper is to present a fairly accurate assessment of the upper bound of the payload capabilities of advanced propulsion vehicles for the various interplanetary missions contemplated within the next decade. Secondly, the nature of advanced propulsion trajectories as they occur both in a planetocentric framework as well as in the heliocentric sphere of influence is described in some detail.

The analysis by which these results were obtained was based upon a two-body inverse-square force field model, generally of two dimensions. Occasional results based upon a three-dimensional analysis are presented, and from these the general effects of non-coplanar orbit transfer may be understood.

To fully appreciate the results contained herein it is necessary to have a fair understanding of the fundamentals of the flight analysis of power-limited propulsion systems. With this in mind, a brief summary of these fundamentals is presented in Section II. The nature of the thrust program employed for the heliocentric transfer region is then discussed in some detail; its advantages and shortcomings are considered. The results of the numerical studies are presented mainly in tabular and graphical form. A particular mission to Jupiter illustrates the manner by which the payload capabilities of a particular vehicle are obtained. These results extend the original work of Irving and Blum (Ref. 1) to a larger class of missions and to three-dimensional trajectories. Appendix A treats the analytical basis of this program.

II. FUNDAMENTALS OF POWER-LIMITED PROPULSION SYSTEMS

The attractiveness of advanced propulsion systems stems from their high specific impulse I_{sp} . Table 1 exhibits the range of I_{sp} and acceleration levels of some propulsion systems presently under consideration.

Unlike the chemical system, for which the source of power for propulsion is contained in the propellants, the advanced propulsion systems currently under study possess a separate power supply to generate the kinetic energy of the propellant. This power supply is necessarily limited in its power output and requires the allocation of a significant percentage of the vehicle weight. These two factors tend to nullify the advantages gained from a high I_{sp} so that tradeoff studies become necessary to determine whether or not an advanced system should be utilized at all for a particular mission, and, if utilized, to optimize the overall configuration of the vehicle in order to obtain maximum payload, or to satisfy some other criterion. These points will become clear in the subsequent discussion.

From Table 1 it is observed that advanced propulsion systems have low thrust acceleration capabilities. The basic reason for this lies in the ability of the system to expend power in the exhaust propellant. In spite of its low I_{sp} , a chemical system typically is capable, through the oxidation of its propellants, of 10^4 more beam or exhaust power than an ion rocket because of the high propellant flow rate. The chemical rocket expels large amounts of propellant in a short time. The advanced system, on the other hand, derives its power from its power supply and is therefore power-limited. If the advanced motor is to maintain its high I_{sp} , it must necessarily regulate its propellant flow rate in order not to exceed the power rating of the power supply. This may be seen quantitatively in the following manner. The thrust F from the exhaust is given by

$$F = \dot{M}_p g I_{sp} = \dot{M}_p c \quad (1)$$

and the power in the beam is given by

$$P = \frac{1}{2} \dot{M}_p c^2 \quad (2)$$

where \dot{M}_p is the mass flow rate of the propellant and c is the exhaust velocity. It is convenient to introduce the quantity α , the specific mass of the powerplant, as

$$\alpha = \frac{M_W}{P} \quad (3)$$

where M_W is the mass of the powerplant and its supporting equipment and P is its power rating. This quantity is quite important in vehicle performance considerations. The relation between beam power and power rating is given by

$$p = \epsilon P \quad (4)$$

where ϵ is the efficiency of the propulsion system in the conversion of power from the supply to kinetic power in the beam. This quantity ϵ for a given engineering design of the propulsion system is, in general, a function of I_{sp} .

The thrust acceleration of the vehicle a may now be written in the form

$$|a| = \frac{F}{M} = \frac{2\epsilon}{\alpha c} \cdot \frac{M_W}{M} \leq \frac{2}{\alpha c} \quad (5)$$

where M is the vehicle mass. The lowest value for α contemplated for powerplant designs in the next decade is around 4 kg/kw. Using a specific impulse of 3000 sec, which is low for the MHD and ion systems, it follows that $\alpha \leq 10^{-3} g$. Thus, it will be seen that the value of α plays a strong role in the thrust acceleration available to an advanced propulsion vehicle. Even a reduction in α by a factor of 10, which might be possible in the next decade, still restricts us to low thrust systems.

A. Rocket Equation for Power-Limited Flight

It will be recalled that the rocket equation for the chemical system is given by

$$M(t) = M_0 \exp \left[- \int_0^t \frac{a}{c} dt \right] \quad (6)$$

where M_0 is the initial vehicle mass. Since the advanced propulsion system has a separate power supply and hence a maximum power level, it is necessary to take cognizance of this constraint in considering its performance. The above expression does not reflect this constraint. A rocket equation suitable for power-limited systems is obtained by combining Eq. (1), (2), and (4) with the expression

$$a = - \frac{F}{M}$$

and integrating over time to obtain

$$\frac{1}{M(t)} = \frac{1}{M_0} + \frac{1}{2P} \int_0^t \frac{a^2}{\epsilon} dt \quad (7)$$

where it has been assumed that the power rating of the power supply is constant with time. This equation will prove instrumental in subsequent performance considerations.

In the case of the chemical system it will be seen that maximum vehicle weight relative to initial weight is attained by choosing a thrust program for a particular mission which minimizes $\int (a/c) dt$. In the case of the power-limited system this is attained by minimizing $\int (a^2/\epsilon) dt$. This will be discussed in more detail later.

B. Allocation of M_L , M_W , and M_p

In order to emphasize the importance of proper allocation of mass among the various vehicle components, consider the variation of gross vehicle payload and structural mass M_L with powerplant mass and $\int_0^T (a^2/\epsilon) dt$, where T is the flight time of the mission. In this regard, the treatment in Ref. 1 will be followed closely. If Eq. (3) is introduced into the rocket equation, it follows that

$$\frac{1}{M(t)} = \frac{1}{M_0} + \frac{\beta^2}{M_W} \quad (8)$$

where β^2 is a dimensionless quantity given by

$$\beta^2(t) = \frac{\alpha}{2} \int_0^t \frac{a^2}{\epsilon} dt \quad (9)$$

This quantity depends upon the flight time T , the mission involved, by which is meant the specification of the kinematic condition of the vehicle at $t = 0$ and $t = T$ (and at any other time which might be necessary), the force field in which the vehicle travels, the kind of thrust program used to accomplish this mission, and, finally, the engineering design of the system as characterized by the quantities α and ϵ . For the present, $\beta^2 \equiv \beta^2(T)$ will be considered as a parameter in the allocating process. At any time the vehicle mass is given by

$$M(t) = M_L + M_W + M_p(t) \quad (10)$$

$M_p(t)$ being the remaining mass of propellant. Now $M_p(0)$ will be assumed to be that amount of propellant required to complete the mission; thus, $M_p(T) = 0$. Placing this into Eq. (8) at $t = T$ there results

$$\frac{M_L}{M_0} = \frac{M_W}{M_0} \left(\frac{1}{\frac{M_W}{M_0} + \beta^2} - 1 \right) \quad (11)$$

and

$$\frac{M_p(0)}{M_0} = \frac{\beta^2}{\frac{M_W}{M_0} + \beta^2} \quad (12)$$

Notice that β^2 must be < 1 for positive M_L . Assume for the moment that β is specified. Then it will be seen that contingent on this value of β there is an optimum allocation of mass to the powerplant which maximizes M_L . From Eq. (11) it may be found that this occurs when

$$\left. \frac{M_W}{M_0} \right|_{\text{optimal}} = \beta(1 - \beta) \quad (13)$$

from which it follows that

$$\left. \frac{M_L}{M_0} \right|_{\text{maximum}} = (1 - \beta)^2 \quad (14)$$

and

$$\frac{M_p(0)}{M_0} = \beta \quad (15)$$

Figures 1 and 2 are plots of M_L/M_0 vs M_W/M_0 for various parametric values of β . It is conceivable that a weak relationship exists between β and M_W/M_0 through a slight dependence of α on M_W/M_0 , in which case these curves will be modified somewhat with a resultant shift in the maxima. For most power systems now being considered α does seem to be fairly independent of M_W/M_0 for a given vehicle size.

C. The Minimization of β

Ultimately, it is seen that the payload capability depends upon the minimization of β . The quantities α and ϵ , as has been seen, depend on the state of the art of the engineering design of the system. Obviously, for optimum performance the quantity ϵ should be as near 1 as possible, particularly for regions requiring high thrust acceleration. This, unfortunately, is usually not at present the case for most designs; ϵ generally drops to low values for low I_{sp} . The optimization of the thrust program must in general take into account this variation of ϵ .

The minimization of $\int_0^T (a^2/\epsilon) dt$ for a specified mission will be seen to be a calculus of variations problem in which this integral is minimized subject to certain constraints, namely, the equations of motion for the vehicle and the specified kinematic conditions of the vehicle to be fulfilled at the initial, terminal, and any other points of the trajectory as required.

This minimization procedure is far from being a pedantic exercise characteristic of some optimization problems; rather, the results of this minimization provide a *modus operandi* for low thrust trajectories with specified end conditions. There are an uncountable number of thrust programs which will accomplish the specified mission, and, of course, the performance of the vehicle can be strongly dependent upon the program utilized. One of the ultimate goals in the design of trajectories is to isolate those types of thrust programs which yield at least near-optimum performances but which are also compatible with the engineering constraints arising from the vehicle and propulsion system design.

The minimization of $\int_0^T (a^2/\epsilon) dt$ will be seen, therefore, to be dependent on the design of the propulsion system, i.e., on the manner in which ϵ varies with I_{sp} . If one is interested in the preliminary design and the systematics of interplanetary power-limited trajectories, then this dependency on ϵ is an undesirable feature and a hindrance. At this stage of our studies it is desirable, instead, to use thrust programs which are independent of this design constraint but which bracket or isolate that class of trajectories and vehicle performances which an actual vehicle would be capable of achieving.

Two such thrust programs which serve this purpose are obtained from the following criteria:

$$\int_0^T a^2 dt = \text{minimum, unconstrained thrust vector}$$

and alternately,

$$\int_0^T a^2 dt = \text{minimum,} \quad \text{thrust magnitude} = \text{constant or 0}$$

The former criterion yields the absolute minimum value that β may have and gives rise to the so-called optimum thrust equations of power-limited flight (cf. Ref. 1, Appendix A). Its justification stems from the fact that over a wide range of I_{sp} (but excluding the lower range, e.g., $I_{sp} < 3000$ sec), ϵ is essentially constant and may therefore be removed from the integral. The second criterion yields the constant thrust equations which minimize $\int a^2 dt$ over

those periods where there is propulsion. The resulting value $\int_0^T a^2 dt$ is always higher than in the first case, but with the judicious use of a coast period along the trajectory it may be reduced in some cases to about 10% more than the first case.¹ In the second case, ϵ is also a constant since the thrust is constant over the trajectory (or zero in the coasting region).

For a particular mission, then, the generation of a pair of trajectories, thrust programs, and vehicle performances using these two criteria would be extremely valuable in determining mission feasibility, payload capability, trajectory design, etc. The first phase of this study, using the optimum thrust equations, is nearly completed, and the results are presented in this paper. The second phase, using the second criterion of constant thrust, will be reported at a later date.

Now consider the optimum thrust equations in detail. It is shown in Appendix A that the differential equations satisfying the criterion that

$$\int_0^T a^2 dt = \text{minimum}$$

and also Newton's laws of motion are given by

$$\ddot{\mathbf{a}} + (\mathbf{a} \cdot \nabla) \nabla V = 0 \quad (16)$$

and

$$\ddot{\mathbf{r}} + \nabla V - \mathbf{a} = 0 \quad (17)$$

where \mathbf{r} is the position vector from an inertial reference and V is the potential of the force field. The gradient operator is taken with respect to position coordinates only, and therefore does not operate on \mathbf{a} , which is a function of time. These vector equations admit a first integral in scalar form which may be written as

$$\dot{\mathbf{a}} \cdot \dot{\mathbf{r}} - \frac{1}{2} a^2 + \mathbf{a} \cdot \nabla V = C \quad (18)$$

This last equation is quite valuable in checking the accuracy of numerical integrations of Eq. (16) and (17).

¹ See Appendix A for a one-dimensional example comparing these two thrust programs.

For the purposes of this study, the confinement of these equations to a two-body inverse-square force field model will suffice. Just as in the case of chemical rocket trajectories, fairly accurate results, particularly in regard to vehicle performances, may be obtained by considering the overall interplanetary trajectory in segments—a geocentric phase, a heliocentric phase, and a planetocentric phase. This procedure is followed here. Even with these simplifications the resulting equations are sufficiently complex that a numerical solution is required.

The great bulk of the numerical results reported here were obtained with a two-dimensional analysis, but occasional three-dimensional results are presented in support of this material. It is possible to assess the effects of the third dimension fairly adequately through these results, although more complete information dealing with the effects of both the planetary orbit inclinations to the ecliptic and eccentricities will be presented at a later date.

III. INTERPLANETARY VEHICLE PERFORMANCE REQUIREMENTS

The discussion now turns to the heliocentric phase of interplanetary trajectories, which extends between the spheres of influence of the departure and target planets. Over all of the heliocentric phase it is assumed that only the Sun's gravitational field need be considered. Thus, at the initial point of the heliocentric phase, the vehicle is assumed to have just escaped from the Earth; therefore, it possesses its kinematic conditions about the Sun.

The two kinds of missions to be considered here are the so-called orbiter and flyby missions. These two missions require markedly different heliocentric thrust programs. In the case of the orbiter, it is necessary because of the low thrust to encounter the target planet with its orbital velocity about the Sun in order for the vehicle to be captured. This, in general, requires a thrust program which is variable in direction or magnitude, or both. The flyby mission requires only that the vehicle encounter the planet and does not, in general,² make any specification about the terminal velocity. The thrust program employed for this case can be simpler and generally has significantly lower propellant requirements.

As stated in Section II, the heliocentric trajectories for both of these mission types will be generated by the optimum thrust program as characterized by Eq. (16) and (17). It will be observed that in three dimensions these equations constitute a twelfth-order system, and thus 12 constants of motion are required for complete specification. These are usually given by the six position and velocity coordinates at the initial point of the trajectory and six other initial quantities whose values are such that the trajectory satisfies the desired terminal conditions. These six additional quantities are customarily $\alpha(0)$ and $\dot{\alpha}(0)$. This leads to the "two-point boundary value problem" which arises whenever analytical solutions to these differential equations are unavailable and values of the variables of the problem are specified at some point other than the initial point. Since these differential equations are solved numerically, an iterative procedure is employed to obtain the values of $\alpha(0)$ and $\dot{\alpha}(0)$, which satisfy the terminal conditions. Iterative procedures are hindered by the extreme sensitivity of some terminal quantities to changes in initial conditions.

A reduction of the dimensionality to two improves the problem. Furthermore, by using a polar coordinate formulation the inherent symmetry of the problem which exists in a central force field aids in reducing the number of required variables. Both the two- and three-dimensional polar coordinate formulations of Eq. (16), (17), and (18)

²The desirability of an encounter with a certain duration will, of course, affect the terminal velocity conditions.

have been programmed for numerical solution on an IBM 7090. These formulations are presented in Appendix A. It will be observed that the heliocentric polar angle θ is a cyclical variable and that the constant K_1 is the resulting constant of motion. If no specification of the terminal value of θ is made, it is shown that K_1 becomes zero, which reduces the number of required initial quantities by one. With K_1 equal to zero, there is no constraint on $\theta(T)$ and the resulting trajectory for a particular mission is an optimum one with respect to $\theta(T)$, since $\int_0^T a^2 dt$ is an extremal for this case. For a particular mission, setting K_1 to zero yields, a one-to-one relation between $\theta(T)$ and T , the heliocentric flight time. Since we are not interested in firing dates in this study and have assumed that the Earth's orbit is circular, it is not necessary to place a constraint on $\theta(T)$.

The two-dimensional polar equations (Eq. A-28 — A-33, Appendix A) with K_1 equal to zero have been coupled with an automatic three-variable iterative routine for selecting the appropriate values of $a_r(0)$, $a_\theta(0)$, and $\dot{a}_r(0)$ which satisfy the specified terminal conditions for a particular mission and heliocentric flight time. This routine possesses a "memory" scheme whereby information concerning the proper values of $a_r(0)$, $a_\theta(0)$, and $\dot{a}_r(0)$ for previous flight times and/or terminal conditions, as well as the matrix coefficients of the iterative routine, is employed to predict the proper values for new flight times and/or terminal conditions. This direct method has been remarkably successful in efficiently obtaining trajectories over a wide range of missions and flight times, which satisfy the required terminal values to at least one part in 10^5 (and in many cases as high as one part in 10^7).

For the orbiter missions the three required terminal conditions in two dimensions are that at $t = T$ (t being zero at heliocentric injection) the heliocentric radius vector $r(T)$ has a specified value and the two components of velocity, which may be expressed in terms of $h(T)$, the angular momentum, and $\dot{r}(T)$, the radial velocity, also have specified values. For the flyby mission, where, at $t = T$ and $r = r(T)$, a specified value, it is shown in Appendix A that optimum performance is obtained by having a trajectory with $a_r(T) = a_\theta(T) = 0$.

For these two mission types, families of trajectories have been obtained which extend over a wide range of heliocentric flight times for the planets Mercury, Venus, Mars, Jupiter, and Saturn. These trajectories all commence with the Earth's heliocentric orbital conditions, which are assumed circular and given by the values

$$\begin{cases} r(0) = 1.494 \times 10^{11} \text{ m} \\ \dot{r}(0) = 0 \\ \theta(0) = 0 \\ h(0) = 4.4497877 \times 10^{15} \text{ m}^2/\text{sec} \end{cases} \quad (19)$$

The value of GM for the Sun was taken as

$$GM = 1.3253421 \times 10^{20} \text{ m}^3/\text{sec}^2$$

Tables 2-11 list the pertinent data for these heliocentric trajectories. The first column is T , the heliocentric flight time in days. The terminal condition column indicates whether the orbit of the target planet was assumed circular or eccentric and, if the latter, where on the orbit rendezvous occurred. The quantity s is the semimajor axis of the planetary orbit about the Sun. For Mercury and Mars, a set of trajectories which rendezvous at the optimum point on the orbit is included. For these trajectories, the value of η , the true anomaly at the interception point, is given. The other columns are self-explanatory. The units employed are meters, seconds, radians, and degrees, if specified. The angle $\psi(0)$ is the angle between the initial thrust acceleration vector and the radius vector; thus, $a_r(0)$ and $a_\theta(0)$ are defined by

$$\left. \begin{aligned} a_r(0) &= a(0) \cos \psi(0) \\ a_\theta(0) &= a(0) \sin \psi(0) \end{aligned} \right\} \quad (20)$$

The quantities $a(0)$, $\psi(0)$, and $\dot{a}_r(0)$ have been included in order to facilitate the duplication of any of the trajectories. If a detailed printout of an overall trajectory is desired, these three quantities, along with the four contained in Eq. (19), and K_1 set to zero, will be required as the eight initial conditions for the numerical solution of Eq. (A-28)–(A-33) of Appendix A.

For vehicle payload capabilities the quantity $\int_0^T a^2 dt$ is required and is listed for each trajectory. This quantity is also plotted vs T for these missions in Fig. 3—9. Figures 4 and 7 exhibit the effects on $\int_0^T a^2 dt$ arising from rendezvousing Mercury and Mars at different points on their eccentric orbits and at the points yielding the minimum value of $\int_0^T a^2 dt$. Figures 10 and 11 exhibit the variation of η with flight time for those trajectories terminating at the optimum interception point. For the other planets the effects of orbital eccentricity are quite small; an example of this can be seen in the case of Jupiter (Fig. 8). This is due to the small eccentricities of the remainder of the planets and, in the case of the major planets, their great distances from the Earth. It will be observed for the orbiter missions that the assumption of circular end conditions leads, as expected, to somewhat higher values of $\int_0^T a^2 dt$ compared with the elliptical cases.

As an example of the manner in which the initial values of $a(0)$, $\psi(0)$, and $\dot{a}_r(0)$ and the quantity $\int_0^T a^2 dt$ vary from one planetary orbit to another, these quantities are plotted (Fig. 12—15, respectively) vs $r(T)$, the heliocentric terminal radius. The trajectories associated with these values all terminate at $r(T)$ with circular conditions and possess a fixed flight time of 178.5 days. The comparatively linear variation of $a(0)$ and $\psi(0)$ with r leads to a fairly efficient search routine with r varying and T fixed. The quantity $\dot{a}_r(0)$, on the other hand, is quite non-linear which, because of the sensitivity of some of the terminal quantities to its value, leads to some complications.

One cautionary remark should be made here. The Euler-Lagrange equations as characterized by Eq. (16) are only necessary conditions that $\int_0^T a^2 dt$ be a minimum; they are not sufficiency conditions. It is possible to have a stationary value of $\int_0^T a^2 dt$ (inflection point) but not a minimum. More important, it is possible to have only a relative minimum and not the absolute minimum value for a particular mission and flight time. That is to say there may be a multiplicity of trajectory paths and thrust programs which are all distinctly different, which all satisfy the Euler-Lagrange equations and the mission and flight time requirements, but which yield significantly different values of $\int_0^T a^2 dt$.

As an example, the reader will recall that the geodesic between two points on a cylinder is a helix between the points. There are, however, two such arcs; the shorter one subtends a polar angle less than 180 deg while the other one is greater than 180 deg.

Several "relative minimum" trajectories have been encountered by the writer, and a particular one is shown in Table 2 for a 360-day Mercury flyby mission. Fortunately, even in the more subtle cases such as the above example, the relative minimum trajectories are fairly easy to detect by the radical departures of their variables from the general trend. Figure 16 exhibits an outstanding example of this effect for a 30-day orbiter flight to Mars. Since K_1 is zero, the shorter path yields a local minimum with respect to $\theta(T)$ and the longer path is a local maximum.

By a combination of continuity methods using curves such as those shown in Fig. 12—15 and the possession of one or more sure "absolute minimum" trajectories it has been concluded that the trajectories presented in Tables 2—11 are "absolute minimum" trajectories.

Unlike chemical vehicle trajectories the effect of departure from coplanarity of the planetary orbits on payload capabilities is very small for advanced propulsion trajectories. This is due to the small planetary inclinations and the relative efficiency with which the advanced system is capable of generating these required inclinations of the trajectory at the terminal point. The planet Mercury shows the greatest effect, as would be expected, because of its 7-deg inclination to the ecliptic.

At present, the three-dimensional iterative routine is incomplete and only isolated trajectories have been obtained which satisfy the three-dimensional terminal requirements of certain missions. A sample of these trajectories is presented in Table 12 for Mercury, Venus, and Mars, for which the effects of the third dimension are most noticeable. It will be observed that the values for $a_r(0)$, $a_\theta(0)$ and $\dot{a}_r(0)$ are almost insignificantly changed by the introduction of the third dimension. This is because the small inclinations involved lead to an almost complete uncoupling of the equations describing the variables in the third dimension from those equations for two dimensions (see Appendix A). It will be observed that the effect of eccentricity is much more pronounced than inclination on $\int_0^T a^2 dt$.

Figures 17 — 19 and 20 — 22 are presented as examples of three-dimensional heliocentric trajectories for 178-day Mars and 120-day Venus orbiter missions, respectively. Figures 17 and 20 are ecliptic projections of the trajectories for these two cases. The arrows on the trajectories indicate the projected direction and magnitude of thrust acceleration. Figures 18 and 21 show the variation of ϕ , the celestial latitude of the vehicle, while Fig. 19 and 22 exhibit the thrust acceleration programs. Figure 23 shows an example of a two-dimensional 510-day Jupiter orbiter and flyby mission.

IV. PLANETOCENTRIC SPIRAL TRAJECTORIES

The planetocentric phases of an interplanetary trajectory – the spiral trajectories – are now considered. This phase is generally defined as including that portion of the trajectory within the sphere of influence of the planet. For our purposes it will be defined as the region containing the commencement from (or termination in, if a capture spiral) a satellite orbit to the point of escape energy. For the range of thrust acceleration now being considered ($10^{-3} - 10^{-6} g$) the escape point lies at a fairly large distance from the planet (Fig. 24) and the transition region between planetocentric and heliocentric phases is transversed quite rapidly. These approximations affect vehicle performance considerations almost insignificantly.

From our previous considerations it follows that the planetocentric portion of interplanetary trajectories, except near escape, are low thrust trajectories for advanced propulsion vehicles. An advanced propulsion vehicle which commences from a satellite orbit generates an outward spiraling trajectory executing many revolutions about the planet before escaping. Figure 24 illustrates such a trajectory for a vehicle possessing an initial acceleration to local gravity ratio of 5×10^{-5} and a specific impulse of 2624 sec. This vehicle commences from an altitude of 200 statute miles ($r = 6.701 \times 10^6 \text{ m}$) above the Earth and employs a tangential thrust program. Because the inner spirals are grouped so closely, only the last few turns are shown in detail.

This trajectory was obtained from the numerical integration of Newton's equations for a two-body inverse-square force field model. These equations have been programmed for numerical solution with various thrust programs and may be expressed generally as

$$\ddot{\mathbf{r}} + \frac{\mu \mathbf{r}}{r^3} - \mathbf{a} = 0 \quad (21)$$

and

$$\mathbf{a} = \mathbf{a}(r, \dot{r}, t) \quad (22)$$

where μ is GM of the central body and $\mathbf{a}(r, \dot{r}, t)$ is a function reflecting the specified thrust program. Equation (22), in effect, replaces Eq. (16) for this phase.

One may easily employ an optimum thrust program, but experience has shown that the improvement in vehicle performance over a straightforward tangential or circumferential constant thrust program is very slight. This is due to the low thrust acceleration to local gravity ratio which exists over all but the last turn of the spiral trajectory. (In the heliocentric phase where this ratio is nearer to 1 and where specified terminal conditions require marked departures from a gravity-turn thrust program, the superiority of the optimum thrust program is quite significant.)

The low thrust acceleration produces only a small perturbation in the vehicle motion about the planet. It is possible by a method of variation of parameters to produce analytic and semiempirical expressions which accurately describe the motion of the vehicle over all the planetocentric trajectory with the exception of the last one or two turns. In Appendix B, several of these expressions are derived and a comparison is made with results obtained with the digital computer. The expressions are extremely accurate for determining vehicle propellant requirements, time to escape, etc.

In this section these formulae are used to show how the vehicle propellant requirement for the planetocentric phase may be determined. From Appendix B it is found that the semimajor axis of the osculating ellipse describing the instantaneous motion of the vehicle under constant tangential thrust (i.e., constant propellant flow rate and I_{sp}) may be expressed as a function of time by the relation

$$s = \frac{r_0}{\left[1 + \frac{1}{\nu} \ln(1 - \nu \tau)\right]^2} \quad (23)$$

where s is the semimajor axis, r_0 is the initial radius of the satellite orbit (assumed circular), ν is a dimensionless parameter related to specific impulse by the expression

$$\nu = \frac{1}{I_{sp} g} \sqrt{\frac{\mu}{r_0}} \quad (24)$$

g being the surface gravity of the Earth, and τ is a dimensionless time variable measured from satellite orbit takeoff and is related to actual time through the relation

$$t = \tau \frac{1}{a_0} \sqrt{\frac{\mu}{r_0}} \quad (25)$$

where a_0 is the initial thrust acceleration. Over all but the last couple of turns the semimajor axis s and the radial distance r , are essentially the same for an initially circular satellite orbit (see Appendix B). For small values of ν which is, in effect, large values of I_{sp} , and therefore an essentially constant vehicle weight with time, Eq. (23) simplifies to

$$s = \frac{r_0}{(1 - \tau)^2} \quad (26)$$

which was obtained by Tsien (Ref. 2). When s reaches infinity the vehicle has attained the velocity of escape, and if ν is negligible it follows from Eq. (25) and (26) that this occurs at

$$T = \frac{\gamma(a_0)}{a_0} \sqrt{\frac{\mu}{r_0}} \quad (\nu = 0) \quad (27)$$

As explained in Appendix B, $\gamma(a_0)$ is a correction term, near 1, which is exhibited in Fig. 25. It was designed to give the exact escape time when $\nu = 0$. It ranges from 1 for very low thrust to $\sqrt{2} - 1$ for infinite thrust and is, in effect, the velocity increment required to escape with a tangential thrust program, expressed as a percentage of the initial circular velocity.

The effect of a finite I_{sp} is to reduce the vehicle weight with time, and thus escape occurs sooner. From Eq. (23) and (25) this is given by

$$T = \frac{1 - e^{-\nu}}{\nu} \frac{\gamma(a_0)}{a_0} \sqrt{\frac{\mu}{r_0}} \quad (28)$$

where the correction term $\gamma(a_0)$ has been included. This expression yields a very accurate determination of escape time. The factor $(1 - e^{-\nu})/\nu$ has been plotted in Fig. 26. For constant thrust acceleration, Eq. (27) holds.

These expressions are applicable to escaping trajectories. Capture trajectories are equivalent to escaping spirals, with the vehicle weight increasing instead of decreasing; therefore, by changing ν to a negative number and measuring time positive from the terminal satellite orbit, these apply also to capture trajectories.

For the thrust program employed here, the propellant consumed in attaining the velocity of escape is given by

$$M_p = \dot{M}_p T \quad (29)$$

The propellant flow rate is given by

$$\dot{M}_p = \frac{M_0 a_0}{I_{sp} g} \quad (30)$$

from which it follows, using Eq. (24) and (28),

$$M_p = M_0 \gamma(a_0) (1 - e^{-\nu}) \quad (31)$$

where M_0 is the initial vehicle mass.

For capture orbits, Eq. (31) becomes

$$M_p = M_0 \gamma(a_0) (e^{+\nu} - 1) \quad (32)$$

where M_0 and a_0 are evaluated at the terminal satellite orbit of the capture spiral.

It also is convenient to have $\int_0^T a^2 dt$ for this case. For constant thrust

$$\int_0^T a^2 dt = \frac{a_0^2 T}{1 - \frac{\dot{M}_p}{M_0} T} \quad (33)$$

which, upon employing Eq. (24) and (28), becomes

$$\int_0^T a^2 dt = \frac{a_0 I_{sp} g \gamma(a_0) (1 - e^{-\nu})}{1 - \gamma(a_0) (1 - e^{-\nu})} \quad (34)$$

For capture spirals, Eq. (34) becomes

$$\int_0^T a^2 dt = \left| \frac{a_0 I_{sp} g \gamma(a_0) (1 - e^{|\nu|})}{1 - \gamma(a_0) (1 - e^{|\nu|})} \right| \quad (35)$$

where a_0 is acceleration at termination in the satellite orbit. For constant thrust acceleration, Eq. (33) becomes

$$\int_0^T a^2 dt = a_0 \gamma(a_0) \sqrt{\frac{\mu}{r_0}} \quad (36)$$

The trajectory exhibited in Fig. 24 has a I_{sp} of 2624 sec and a value $\nu = 0.300$. The tabulation below gives a comparison between Eq. (28), (31), and (34) and their exact values.

	Analytic	Exact
$T \times 10^{-7} \text{ S}$	1.3992	1.4067
M_p / M_0	0.24156	0.24286
$\int_0^T a^2 dt, \text{ m}^2/\text{sec}^3$	3.6344	3.6603

The value of ν is rather high for most interplanetary vehicle systems now being considered but was chosen here to illustrate the general validity of these expressions.

It follows from Eq. (31) or (34) and (24) that to the first order the vehicle propellant requirements for the planetocentric phases are proportional, for a given I_{sp} , to the satellite orbital velocity $\sqrt{\mu/r_0}$. Table 13 lists the equatorial radii R and the orbital velocities of various altitude orbits above the equatorial surface of the planets. The large propellant requirement for spiralling around the major planets can be lessened considerably by termination in a highly elliptical satellite orbit with a low perigee distance.

V. NUMERICAL EXAMPLE OF VEHICLE PAYLOAD CAPABILITIES

Consider a mission to Jupiter employing an advanced propulsion vehicle coupled with a chemical booster capable of placing 8,000 kg of useful payload into a 200-mile orbit about the Earth. The specific mass of the powerplant is taken as $\alpha = 4$ kg/kw. As a first iteration it is assumed that the powerplant constitutes $\frac{1}{4}$ of the total vehicle mass, which leads to a powerplant mass of 2000 kg and a power rating of 500 kw. For the geocentric phase, the escape time is nearly inversely proportional to the thrust acceleration. Thus, a thrust as high as that which is compatible with propellant consumption and the engineering design of the propulsion system should be used to minimize the escape time. For this case, assume an I_{sp} of 5000 sec at an electrical power conversion efficiency of $\epsilon = 0.5$. This leads to an initial acceleration of

$$a_0 = 1.28 \times 10^{-3} \text{ m/sec}^2$$

and a propellant flow rate of

$$\dot{M}_p = 2.08 \times 10^{-4} \text{ kg/sec}$$

From Eq. (24) one finds ν to be

$$\nu = 0.157$$

From Eq. (28) it will be found that the escape time for this trajectory

$$T_e = 5.35 \times 10^6 = 62 \text{ days}$$

The value of $\int_0^{T_e} a^2 dt$ and the propellant consumption for the geocentric phase are

$$\int_0^{T_e} a^2 dt = 10.1 \text{ m}^2/\text{sec}^3$$

and

$$M_p = \dot{M}_p T_e = 1,110 \text{ kg}$$

leaving a vehicle mass at heliocentric injection of 6890 kg.

For the heliocentric phase, a flight time of $T_H = 510$ days is selected. For the orbiter mission, $\int_0^T a^2 dt = 39.3 \text{ m}^2/\text{sec}^3$ while for the flyby, $\int_0^T a^2 dt = 9.45 \text{ m}^2/\text{sec}^3$. Figure 23 shows these two trajectories. The thrust acceleration at heliocentric injection for the orbiter for optimum performance is $1.6 \times 10^{-3} \text{ m/sec}^2$; this is comparable with the geocentric acceleration which at geocentric escape is $1.5 \times 10^{-3} \text{ m/sec}^2$. The initial flyby acceleration is only $6.8 \times 10^{-4} \text{ m/sec}^2$; furthermore, the thrust acceleration over the remainder of the heliocentric phase never exceeds the initial level in the orbiter trajectory. For the heliocentric phase, assuming an average efficiency of $\epsilon = 0.75$, one finds the vehicle mass at the heliocentric terminal point to be

$$M(T_e + T_H) = 5060 \text{ kg, orbiter}$$

$$M(T_e + T_H) = 6350 \text{ kg, flyby}$$

A comparison is made between these mission capabilities and those of a chemical vehicle commencing from a 200-mile geocentric orbit. Assume that the vehicle travels on a heliocentric transfer ellipse to Jupiter in 570 days. Generating this transfer ellipse requires a velocity increment in a 200-mile geocentric orbit of 7.0 km/sec. If one assumes no staging and an I_{sp} of 400 sec for this system, the propellant required is 83% of the initial weight. Further, for the orbiter mission, a second velocity increment to effect capture by Jupiter must be added. The magnitude of this increment must be at least sufficient to cancel the relative hyperbolic velocity of 2 km/sec. However, because of Jupiter's large mass it is particularly advantageous to apply this retro maneuver near perigee of the incoming hyperbola where only a small fraction of this 2 km/sec increment is required to obtain a highly elliptic orbit about Jupiter. If 50% of the remaining vehicle weight after departure from the Earth-satellite orbit is assumed to be useful gross payload containing the required retro motor for capture, then after the retro maneuver approximately 8% of the initial vehicle remains as gross payload, structures, and the empty propulsion system. Table 14 gives a comparison of final vehicle weight percentages for the chemical and advanced systems. In the advanced system, the final vehicle weight minus powerplant for the flyby mission may be increased slightly by choosing a powerplant of approximately 15% the initial vehicle weight since β is 0.19 for this mission. For the orbiter, without considering the capture spiral, β is about 0.4, from which it follows from Eq. 13 that the initial choice of M_W/M_0 is about optimum.

The high mass of Jupiter creates a prohibitive propellant requirement in the attainment of a circular satellite orbit near its surface. It may be shown for the above system that the final vehicle weight minus powerplant reduces to 25% of the initial weight if it is placed in an eccentric orbit with a perigee distance and a semimajor axis of 1 and 16 Jupiter radii, respectively. This orbit has a period of about 6 days.

ACKNOWLEDGMENT

The author wishes to express his appreciation to D. E. Richardson and C. M. Warden of the JPL Applied Mathematics Section and to Mrs. Helen Ling of the Systems Analysis Section for their help in obtaining the numerical results.

REFERENCES

1. Irving, J., *Space Technology*, H. Seifert, ed., John Wiley and Sons, Inc., New York, 1959, ch. 10.
2. Tsien, H. S., "Take-off from Satellite Orbits," *Journal of the American Rocket Society*, vol. 23, July - August 1953, pp. 233-236.

Table 1. Specific impulse and thrust acceleration of several propulsion systems

Propulsion type	I_{sp} , sec	Thrust acceleration, g
Chemical	200 – 500	0.01 – 10
Plasma arc heating	400 – 2000	10^{-4} – 10^{-2}
Plasma (MHD)	1500 – 25,000	10^{-5} – 10^{-3}
Ion	3000 – 60,000	10^{-6} – 10^{-4}

Table 2. Mercury orbiter trajectories

T , day	Terminal condition	$\int_0^T a^2 dt$ m^2/sec^3	$\theta(T)$, rad	$a(0)$, m/sec^2	$\psi(0)$, rad	$\dot{a}_r(0)$, m/sec^3
circular						
30		5.1443×10^3	1.2326	7.9534×10^{-2}	3.3512	5.5950×10^{-8}
45		1.3815	1.7661	3.4252	3.4811	1.4751
60		5.2795×10^2	2.2744	1.8558	3.6116	5.4149×10^{-9}
75		2.4754	2.7702	1.1385	3.7363	2.3602
90		1.3424	3.2590	7.5422×10^{-3}	3.8522	1.1376×10^{-9}
105		8.2066×10^1	3.7434	5.2617	3.9581	5.8548×10^{-10}
120		5.5768	4.2247	3.8112	4.0532	3.1739
135		4.1584	4.7041	2.8437	4.1364	1.8182
150		3.3496	5.1834	2.1781	4.2062	1.1207
165		2.8637	5.6654	1.7125	4.2608	7.6203×10^{-11}
180		2.5552	6.1553	1.3874	4.2980	5.7949
195		2.3458	6.6625	1.1672	4.3164	4.8652
210		2.1907	7.2054	1.0328	4.3170	4.3565
240		1.9346	8.6056	1.0155	4.2950	3.6407
270		1.6320	10.361	1.0726×10^{-3}	4.3436	2.3891
300		1.3851	11.474	8.6775×10^{-4}	4.4098	1.4285
330		1.2308	12.454	6.8078	4.4520	1.1348
360		1.1321	13.490	5.6565	4.4580	1.1087
375		1.0926×10^1	14.088	5.4317	4.4485	1.0760×10^{-11}
elliptical						
30	$r = s, \dot{r} = -$	4.1556×10^3	1.0767	7.2944×10^{-2}	3.3774	5.0184×10^{-8}
30	$r = s(1 + e/2), \dot{r} = -$	3.9756	0.98589	7.0136	3.3748	4.9358
30	apogee	4.4285	0.97316	7.1245	3.3557	5.2326
60	$r = s, \dot{r} = -$	4.0395×10^2	1.9261	1.6107	3.6490	4.6509×10^{-9}
60	$r = s(1 + e/2), \dot{r} = -$	4.3340	1.8373	1.6121	3.6267	4.8887
60	apogee	5.7792	1.9489	1.7955	3.5752	5.7663

Table 2 (Cont'd)

T , day	Terminal condition	$\int_0^T a^2 dt$ m^2/sec^3	$\theta(T)$, rad	$a(0)$, m/sec^2	$\psi(0)$, rad	$\dot{a}_r(0)$, m/sec^3
90	elliptical $r = s, \dot{r} = -$	1.1466×10^2	2.7258	6.3565×10^{-3}	3.8785	9.9451×10^{-10}
90	$r = s(1 + e/2), \dot{r} = -$	1.3377	2.6767	6.6891	3.8356	1.1271
90	apogee	1.8078	2.9978	8.1548	3.7799	1.4133×10^{-9}
120	$r = s, \dot{r} = -$	5.8989×10^1	3.5275	3.2424×10^{-3}	4.0423	3.1757×10^{-10}
120	$r = s(1 + e/2), \dot{r} = -$	6.8944	3.5633	3.6521	3.9871	3.8185
120	apogee	7.7433	4.2848	4.8390	3.9681	4.6647
150	$r = s, \dot{r} = -$	4.1901	4.3927	2.0348	4.1304	1.4526
150	$r = s(1 + e/2), \dot{r} = -$	4.5541	4.6375	2.5289	4.0864	1.7361
150	apogee	3.6517	5.9477	3.0177	4.1847	1.4522
165 ^a	apogee	2.7795	6.4336	2.1868×10^{-3}	4.2927	7.0893×10^{-11}
165 ^a	$r = s(1 + e/2), \dot{r} = -$	3.7372	6.5515	2.9866×10^{-3}	4.1688	1.4913×10^{-10}
165 ^a	$r = s, \dot{r} = -$	3.7249	4.9065	1.7858×10^{-3}	4.1485	1.1123×10^{-10}
180	$r = s, \dot{r} = -$	3.3188	5.7332	1.8656	4.1560	9.4576×10^{-11}
180	apogee	2.3244	6.8247	1.5782	4.3908	3.7915
195	apogee	2.0867	7.1783	1.1434	4.4759	2.6754
210	apogee	1.9611	7.5136	8.3537×10^{-4}	4.5404	2.5913
240	apogee	1.8586	8.1664	4.7849	4.5538	3.2848
270	apogee	1.8113×10^1	8.8606	3.7544	4.3564	3.6247
	optimum rendezvous η^0 , true anomaly					
45	- 110.498	1.0626×10^3	1.4774	3.0191×10^{-2}	3.5129	1.2889×10^{-8}
60	- 81.593	398.96	2.0331	1.6348	3.6594	4.5765×10^{-9}
75	- 51.668	182.69	2.6376	9.9394×10^{-3}	3.8040	1.8871×10^{-9}
90	- 22.628	97.481	3.2643	6.4745	3.9415	8.4226×10^{-10}
105	5.457	59.754	3.8932	4.4170	4.0706	3.9184×10^{-10}

^a See Table 12 for a comparison with three-dimensional trajectories.

Table 2. (Cont'd)

T , day	Terminal condition	$\int_0^T a^2 dt$ m^2/sec^3	$\theta(T)$, rad	$a(0)$, m/sec^2	$\psi(0)$, rad	$\dot{a}_r(0)$, m/sec^3
	optimim rendezvous η^o , true anomaly					
120	33.127	41.622	4.5122	3.1211×10^{-3}	4.1908	1.8705×10^{-10}
135	60.661	32.309	5.1097	2.2768	4.3005	9.2809×10^{-11}
150	87.942	27.200	5.6722	1.7200	4.3955	5.0651×10^{-11}
165	114.588	24.172	6.1889	1.3565	4.4687	3.3247×10^{-11}
180	140.268	22.197	6.6612	1.1275	4.5120	2.7188×10^{-11}
210	-169.009	19.565	7.5746	9.3411×10^{-4}	4.5079	2.5332×10^{-11}
240	-96.394	17.216	8.8723	1.0022×10^{-3}	4.4681	1.9506×10^{-11}
270	8.744	14.613	10.724	9.4142×10^{-4}	4.5377	6.0116×10^{-12}
300	83.343	12.790	12.077	7.3667	4.6319	1.3158×10^{-12}
330	141.017	11.649	13.079	6.0243	4.6815	1.9218×10^{-12}
360	-168.005	10.811	13.970	5.4564	4.6696	3.1189×10^{-12}

Table 3. Venus orbiter trajectories

T , day	Terminal condition	$\int_0^T a^2 dt$, m^2/sec^3	$\theta(T)$, rad	$a(0)$, m/sec^2	$\psi(0)$, rad	$\dot{a}_r(0)$, m/sec^3
	circular					
30		1.1359×10^3	0.67583	3.6681×10^{-2}	3.3486	2.6874×10^{-8}
45		3.2250×10^2	1.0100	1.6162	3.4559	7.3986×10^{-9}
60		1.2866×10^2	1.3417	8.9760×10^{-3}	3.5643	2.8124×10^{-9}
75		6.1653×10^1	1.6712	5.6470	3.6714	1.2557×10^{-9}
90		3.3158×10^1	1.9993	3.8374	3.7754	6.1129×10^{-10}
105		1.9343×10^1	2.3265	2.7460	3.8750	3.1060×10^{-10}
120 ^a		1.2020×10^1	2.6531	2.0382	3.9693	1.5950×10^{-10}
135		7.8802	2.9792	1.5543	4.0581	8.0188×10^{-10}
150		5.4249	3.3050	1.2099×10^{-3}	4.1414	3.7744×10^{-10}
165		3.9137	3.6306	9.5730×10^{-4}	4.2189	1.5133×10^{-11}
180		2.9556	3.9561	7.6757	4.2908	3.5081×10^{-12}
195		2.3330	4.2813	6.2243	4.3567	-1.9478×10^{-12}
210		1.9196	4.6065	5.0984	4.4162	-3.9486×10^{-12}
225		1.6397	4.9316	4.2157	4.4688	-4.0625×10^{-12}
240		1.4468	5.2567	3.5197	4.5135	-3.2119×10^{-12}
255		1.3109	5.5819	2.9690	4.5493	-1.9424×10^{-12}
270		1.2132	5.9073	2.5344	4.5749	-5.7855×10^{-13}
285		1.1411	6.2332	2.1947	4.5894	$+6.8855 \times 10^{-13}$
300		1.0861	6.5600	1.9343	4.5920	1.7489×10^{-12}
315		1.0425	6.8881	1.7418	4.5835	2.5427×10^{-12}
330		1.0063	7.2181	1.6083	4.5659	3.0418×10^{-12}
345		0.97467	7.5508	1.5261	4.5431	3.2411×10^{-12}
360		0.94537	7.8873	1.4875	4.5198	3.1526×10^{-12}
375		0.91686	8.2282	1.4841×10^{-4}	4.5007	2.8050×10^{-12}

^a See Table 12 for a comparison with three-dimensional trajectories.

Table 4. Mars orbiter trajectories

T , day	Terminal condition	$\int_0^T a^2 dt$, m^2/sec^3	$\theta(T)$, rad	$a(0)$, m/sec^2	$\psi(0)$, rad	$\dot{a}_r(0)$, m/sec^3
circular						
30		4.1718×10^3	0.39477	6.9775×10^{-2}	0.22375	-5.1382×10^{-8}
60		502.98	0.7849	1.7324	0.42998	-5.5501×10^{-9}
90		140.97	1.1688	7.6064×10^{-3}	0.61122	-1.2817×10^{-9}
119.5			1.5406	4.2436	0.76615	-3.7573×10^{-10}
149.8			1.9169	2.6452	0.90520	-1.0044×10^{-10}
179.64		14.013	2.2908	1.7807	1.0288	-8.6363×10^{-12}
210		8.0601	2.6666	1.2582	1.1410	$+2.1806 \times 10^{-11}$
240		5.0101	3.0270	9.2534	1.2414	2.9144×10^{-11}
270.046		3.3165	3.4074	6.9847×10^{-4}	1.3328	2.7855×10^{-11}
elliptical						
30	$r = s, \dot{r} = -$	3.8657×10^3	0.39703	6.8030×10^{-2}	0.22726	-4.9396×10^{-8}
30	$r = s, \dot{r} = -$	4.4902	0.39143	7.1512	0.21946	-5.3356
30	$r = s(1-e/2), \dot{r} = +$	2.8847	0.41071	5.8764	0.22990	-4.2674
30	$r = s(1-e/2), \dot{r} = -$	3.3756	0.40506	6.1927	0.22128	-4.6268
30	perigee	2.2238	0.42376	5.0843×10^{-2}	0.22928	-3.7514
60	$r = s, \dot{r} = +$	429.86	0.79475	1.6442	0.44358	-5.0800×10^{-9}
60	$r = s, \dot{r} = -$	582.00	0.77349	1.8198	0.41658	-6.0132
60	$r = s(1-e/2), \dot{r} = +$	321.79	0.82200	1.4199	0.44796	-4.3995
60	$r = s(1-e/2), \dot{r} = -$	441.54	0.80067	1.5792	0.41858	-5.2437
60	perigee	273.14	0.84252	1.2660	0.4373	-4.0969
90	$r = s, \dot{r} = +$	110.53	1.1907	7.0092×10^{-3}	0.63777	-1.0970
90	$r = s(1-e/2), \dot{r} = +$	83.617	1.2312	6.0563	0.6420	-9.595×10^{-10}
90	perigee	79.148	1.2545	5.5881	0.61622	-9.7020
120	$r = s, \dot{r} = +$	39.753	1.5852	3.7473	0.80826	-2.8431
120	$r = s(1-e/2), \dot{r} = +$	30.703	1.6385	3.2442	0.81038	-2.5606
120	perigee	32.689	1.6605	3.1144	0.76862	-2.9318

Table 4 (Cont'd)

T , day	Terminal condition	$\int_0^T a^2 dt$, m^2/sec^3	$\theta(T)$, rad	$a(0)$, m/sec^2	$\psi(0)$, rad	$\dot{a}_r(0)$, m/sec^3
	elliptical					
150	$r = s, \dot{r} = +$	17.213	1.9798	2.2573×10^{-3}	0.95087	-6.1769×10^{-11}
150	$r = s(1-e/2), \dot{r} = +$	13.757	2.0451	1.9626	0.95623	-6.1836×10^{-11}
150	perigee	16.476	2.0615	1.9719	0.90009	-8.9248×10^{-11}
180	$r = s, \dot{r} = +$	8.4757	2.3758	1.0114	1.2149	-7.8094×10^{-12}
180	$r = s(1-e/2), \dot{r} = +$	7.1127	2.4518	1.2800	1.0831	-2.6871×10^{-12}
178.5 ^a	perigee	9.7146	2.4384	1.3776	1.0098	-1.9885×10^{-11}
180	perigee	9.4702	2.4584	1.3537	1.0153	-1.7727×10^{-11}
210	$r = s, \dot{r} = +$	4.6527	2.7742	9.9092×10^{-4}	1.2086	2.1202×10^{-11}
210	$r = s(1-e/2), \dot{r} = +$	4.1483	2.8593	8.7918	1.1933	1.3838×10^{-11}
210	perigee	5.9896	2.8511	9.8301	1.1174	8.4734×10^{-12}
240	$r = s, \dot{r} = +$	2.8394	3.1756	6.9459	1.3134	2.1684×10^{-11}
240	perigee	4.0801	3.2396	7.4430	1.2086	1.7276×10^{-11}
270	$r = s, \dot{r} = +$	1.9274	3.5800	4.9939	1.4041	1.7139×10^{-11}
270	$r = s(1-e/2), \dot{r} = +$	1.9354	3.6757	4.6400	1.3674	1.3629×10^{-11}
270	perigee	2.9511	3.6234	5.8223	1.2904	1.9016×10^{-11}
300	$r = s, \dot{r} = +$	1.4463	3.9872	3.6730	1.4787	1.1747×10^{-11}
300	$r = s(1-e/2), \dot{r} = +$	1.5069	4.0832	3.5384	1.4306	1.0265×10^{-11}
300	perigee	2.2425	4.0020	4.6761	1.3641	1.7884×10^{-11}
330	$r = s, \dot{r} = +$	1.1803	4.3963	2.7686	1.5336	7.0280×10^{-12}
330	$r = s(1-e/2), \dot{r} = +$	1.2502	4.4889	2.7888	1.4773	7.2193×10^{-12}
330	perigee	1.7759	4.3752	3.8377	1.4304	1.5672×10^{-11}
360	$r = s, \dot{r} = +$	1.0252	4.8061	2.1522	1.4648	3.4544×10^{-12}
360	$r = s(1-e/2), \dot{r} = +$	1.0855	4.8912	2.2768	1.5082	4.8795×10^{-12}
360	perigee	1.4561	4.7428	3.2063	1.4903	1.3154×10^{-11}
390	$r = s, \dot{r} = +$	0.92797	5.2147	1.7429	1.5703	1.0684×10^{-12}

^a See Table 12 for a comparison with three-dimensional trajectory.

Table 4 (Cont'd)

T , day	Terminal condition	$\int_0^T a^2 dt$, m^2/sec^3	$\theta(T)$, rad	$a(0)$, m/sec^2	$\psi(0)$, rad	$\dot{a}_r(0)$, m/sec^3
	elliptical					
390	$r = s(1-e/2), \dot{r} = +$	0.97185	5.2887	1.9282×10^{-4}	1.5259	3.2656×10^{-12}
390	perigee	1.2297	5.1046	2.7174	1.5441	1.0656×10^{-11}
420	$r = s, \dot{r} = +$	0.86121	5.6202	1.4847	1.5540	-2.7495×10^{-13}
420	$r = s(1-e/2), \dot{r} = +$	0.88754	5.6802	1.6913	1.5351	$+2.2492 \times 10^{-12}$
420	perigee	1.0652	5.4611	2.3237	1.5923	8.3015×10^{-12}
450	$r = s, \dot{r} = +$	0.81021	6.0206	1.3342	1.5267	-8.0350×10^{-13}
450	$r = s(1-e/2), \dot{r} = +$	0.82072	6.0649	1.5280	1.5407	1.6530×10^{-12}
450	perigee	0.94353	5.8131	2.0113	1.6350	6.1240×10^{-12}
	optimum rendezvous η^0 , true anomaly					
60	19.174	264.23	0.84356	1.2598×10^{-2}	0.44333	-4.0146×10^{-9}
75	24.021	131.07	1.0512	8.0070×10^{-3}	0.54100	-1.8305×10^{-9}
90	28.844	73.144	1.2574	5.5128×10^{-3}	0.63257	-9.1574×10^{-10}
105	33.625	44.244	1.4620	4.0081×10^{-3}	0.71836	-4.8120×10^{-10}
120	38.363	28.382	1.6652	3.0306×10^{-3}	0.79886	-2.5706×10^{-10}
135	43.030	19.056	1.8671	2.3601×10^{-3}	0.87453	-1.3505×10^{-10}
150	47.621	13.275	2.0677	1.8802×10^{-3}	0.94581	-6.6410×10^{-11}
165	52.132	9.5413	2.2672	1.5252×10^{-3}	1.01308	-2.7182×10^{-11}
180	56.556	7.0497	2.4655	1.2553×10^{-3}	1.0767	-4.8428×10^{-12}
195	60.894	5.3423	2.6627	1.0456×10^{-3}	1.1368	7.5247×10^{-12}
210	65.140	4.1464	2.8588	8.7952×10^{-4}	1.1937	1.3897×10^{-11}
225	69.293	3.2932	3.0539	7.4606×10^{-4}	1.2475	1.6634×10^{-11}
240	73.346	2.6751	3.2481	6.3737×10^{-4}	1.2982	1.7177×10^{-11}
255	77.278	2.2213	3.4413	5.4789×10^{-4}	1.3459	1.6418×10^{-11}

Table 4 (Cont'd)

T , day	Terminal condition	$\int_0^T a^2 dt$ m^2/sec^3	$\theta(T)$, rad	$a(0)$, m/sec ²	$\psi(0)$, rad	$\dot{a}_r(0)$, m/sec ³
	optimum rendezvous η° , true anomaly					
270	81.106	1.8841	3.6338	4.7352×10^{-4}	1.3904	1.4919×10^{-11}
300	88.357	1.4395	4.0169	3.5873×10^{-4}	1.4694	1.1001×10^{-11}
330	94.724	1.1803	4.3991	2.7638×10^{-4}	1.5326	6.9899×10^{-12}
360	99.915	1.0240	4.7840	2.1665×10^{-4}	1.5750	3.5214×10^{-12}
390	102.868	0.92604	5.1780	1.7393×10^{-4}	1.5888	8.8752×10^{-13}
420	101.289	0.86049	5.5934	1.4632×10^{-4}	1.5660	-6.1436×10^{-13}

Table 5. Jupiter orbiter trajectories

T , day	Terminal condition	$\int_0^T a^2 dt$, m^2/sec^3	$\theta(T)$, rad	$a(0)$, m/sec^2	$\psi(0)$, rad	$\dot{a}_r(0)$, m/sec^3
circular						
180		1.1058×10^3	1.3495	1.5019×10^{-2}	1.0270	1.9714×10^{-10}
240		441.43	1.6693	8.2656×10^{-3}	1.1828	3.6374
300		215.25	1.9641	5.1755	1.2983	2.9861
360		119.54	2.2447	3.5196	1.3896	2.2361
420		72.825	2.5164	2.5353	1.4654	1.6530
480		47.596	2.7821	1.9052	1.5303	1.2255
540		32.904	3.0434	1.4788	1.5871	9.1221×10^{-11}
600		23.833	3.3010	1.1774	1.6372	6.7941
660		17.968	3.5557	9.5698×10^{-4}	1.6812	5.0355
720		14.030	3.8079	7.9110	1.7195	3.6869
780		11.306	4.0583	6.6338	1.7521	2.6397
840		9.3600	4.3072	5.6314	1.7787	1.8188
900		7.9462	4.5554	4.8322	1.7990	1.1714
elliptical						
180	$r = s, \dot{r} = +$	1.0869×10^3	1.3519	1.4935×10^{-2}	1.0285	2.0145×10^{-10}
180	perigee	974.70	1.3684	1.4106	1.0260	1.6490
360	$r = s, \dot{r} = +$	115.25	2.2532	3.4762×10^{-3}	1.3924	2.2097
360	perigee	105.37	2.2914	3.3017	1.3905	2.0646
540	$r = s, \dot{r} = +$	31.195	3.0624	1.4494	1.5910	8.8796×10^{-11}
540	perigee	29.186	3.1195	1.3858	1.5909	8.3997
720	$r = s, \dot{r} = +$	13.180	3.8420	7.6910×10^{-4}	1.7237	3.4968
720	perigee	12.627	3.9125	7.4056	1.7243	3.3182
900	$r = s, \dot{r} = +$	7.4682	4.6093	4.6606	1.8008	1.0319×10^{-11}
900	perigee	7.2976	4.6876	4.5225×10^{-4}	1.8009	9.6943×10^{-12}

Table 6. Saturn orbiter trajectories

T , day	Terminal conditions (circular)	$\int_0^T a^2 dt$, m^2/sec^3	$\theta(T)$, rad	$a(0)$, m/sec^2	$\psi(0)$, rad	$\dot{a}_r(0)$, m/sec^3
180		4.7507×10^3	1.2082	3.0883×10^{-2}	1.0386	9.2128×10^{-10}
240		1.9265×10^3	1.4545	1.7112	1.1910	1.0227×10^{-9}
300		951.75	1.6696	1.0784	1.3006	7.7601×10^{-10}
360		533.98	1.8668	7.3781×10^{-3}	1.3839	5.6356
420			2.0476	5.3454	1.4503	4.1188
480		214.92	2.2317	4.0401	1.5051	3.0610
540		148.49	2.4055	3.1548	1.5517	2.3147
600		106.97	2.5756	2.5281	1.5922	1.5922
660		79.761	2.7428	2.0690	1.6279	1.3817
720		61.224	2.9075	1.7232	1.6596	1.0845
780		48.181	3.0703	1.4566	1.6882	8.5674×10^{-11}
840		38.748	3.2312	1.2468	1.7138	6.7929
900		31.762	3.3907	1.0788	1.7368	5.3888

Table 7. Mercury flyby trajectories (apogee encounter)

$T, \text{ day}$	$\int_0^T a^2 dt$ m^2/sec^3	$\dot{r}(T), \text{m}^2/\text{sec}$	$h(T), \text{m}^2/\text{sec}$	$\theta(T), \text{rad}$	$a(0), \text{m}/\text{sec}^2$	$\psi(0), \text{rad}$	$\dot{a}_r(0), \text{m}/\text{sec}^3$
30	940.05	-5.2606×10^4	2.3413×10^{15}	0.55013	3.4450×10^{-2}	-2.6548	1.1228×10^{-8}
45	240.14	-3.8453	2.5917	0.87253	1.4629×10^{-2}	-2.4532	2.5393×10^{-9}
60	87.013	-3.0511	2.8424	1.2263	7.7532×10^{-3}	-2.2823	7.1061×10^{-10}
75	39.021	-2.4559	3.0578	1.6032	4.6476	-2.1365	1.9030×10^{-10}
90	20.457	-1.9477	3.2265	1.9967	3.0230	-2.0084	2.2147×10^{-11}
105	12.169	-1.4929	3.3493	2.4032	2.0842	-1.8905	-3.3281×10^{-11}
120	8.0746	-1.0826	3.4316	2.8195	1.4962	-1.7741	-4.8829×10^{-11}
135	5.9156	-7.2241×10^3	3.4792	3.2390	1.0979	-1.6478	-4.9066×10^{-11}
150	4.7489	-4.3126	3.4995	3.6460	8.0543×10^{-4}	-1.4947	-4.2450×10^{-11}
165	4.1308	-2.2955	3.5033	4.0176	5.7917	-1.2906	-3.1905×10^{-11}
180	3.8171	-1.1485×10^3	3.5020	4.3393	4.0938	-1.0050	-1.9217×10^{-11}
210	3.5644	-425.63	3.5060	4.8550	2.4639	-0.14179	5.5518×10^{-12}
240	3.4157	-452.28	3.5216	5.2678	2.4533	0.62901	2.3157×10^{-11}
270	3.2444	-587.11	3.5435	5.6253	2.6675	1.0577	3.2661×10^{-11}
300	3.0545	-673.28	3.5680	5.9480	2.7154	1.3314	3.5914×10^{-11}
330	2.8690	-690.71	3.5929	6.2457	2.6151	1.5426	3.4969×10^{-11}
360	2.7036	-654.09	3.6171	6.5249	2.4244	1.7276	3.1421×10^{-11}
360 ^a	3.4775	-1.9603×10^3	3.4767	8.1037	3.8454	-2.0061	-8.2552×10^{-12}

^a Relative minimum trajectory.

Table 8. Venus flyby trajectories

$T, \text{ day}$	$\int_0^T a^2 dt$ m^2/sec^3	$\dot{r}(T), \text{ m/sec}$	$h(T), \text{ m}^2/\text{sec}$	$\theta(T), \text{ rad}$	$a(0), \text{ m/sec}^2$	$\psi(0), \text{ rad}$	$\dot{a}_r(0), \text{ m/sec}^3$
30	26.125	-2.6003×10^4	3.3509×10^{15}	0.5283	1.8007×10^{-2}	-2.6550	5.7039×10^{-9}
60	25.335	-1.4551	3.6060	1.1011	4.1495×10^{-3}	-2.2888	3.5255×10^{-10}
90	5.9728	-9.8313×10^3	3.8133	1.7096	1.6512	-2.0310	9.2878×10^{-12}
120	2.2250	-6.6340	3.9409	2.3367	8.3506×10^{-4}	-1.8339	-2.4682×10^{-11}
150	1.1421	-4.1695	4.0084	2.9760	4.8434	-1.6598	-2.2035×10^{-11}
180	0.75347	-2.2571	4.0354	3.6211	2.9910	-1.4737	-1.4659×10^{-11}
210	0.60604	-9.4200×10^2	4.0378	4.2523	1.7999	-1.2216	-6.5408×10^{-12}
240	0.55689	-2.8220×10^2	4.0330	4.8358	9.6993×10^{-5}	-0.78067	1.5722×10^{-12}
270	0.54295	-9.4501×10^1	4.0339	5.3564	5.5827	-0.077287	8.1787×10^{-12}
300	0.53558	-9.1932×10^1	4.0429	5.8284	5.4446	0.98190	1.2078×10^{-11}
330	0.52726	-1.0665×10^2	4.0567	6.2737	5.7747	1.5516	1.3129×10^{-11}
360	0.51912	-9.2791×10^1	4.0711	6.7139	5.3075×10^{-5}	2.0900	1.1669×10^{-11}

Table 9. Mars flyby trajectories (mean distance encounter)

$T, \text{ day}$	$\int_0^T a^2 dt$ m^2/sec^3	$\dot{r}(T), \text{ m/sec}$	$h(T), \text{ m}^2/\text{sec}$	$\theta(T), \text{ rad}$	$a(0), \text{ m/sec}^2$	$\psi(0), \text{ rad}$	$\dot{a}_r(0), \text{ m/sec}^3$
30	980.38	4.6990×10^4	6.5402×10^{15}	0.50611	3.4453×10^{-2}	0.48572	-1.0404×10^{-8}
60	103.24	2.4855	6.0790	0.96987	8.2032×10^{-3}	0.84548	-5.6386×10^{-10}
90	25.451	1.6989	5.6879	1.3970	3.3900	1.0879	1.9471×10^{-11}
120	9.2737	1.2588	5.4203	1.8046	1.7640	1.2585	6.3333×10^{-11}
150	4.3390	9.6351×10^3	5.2478	2.2019	1.0512	1.3883	5.1233×10^{-11}
180	2.4357	7.4633	5.1388	2.5926	6.8651×10^{-4}	1.4945	3.6526×10^{-11}
210	1.5733	5.7789	5.0718	2.9778	4.7860	1.5864	2.5195×10^{-11}
240	1.1354	4.4306	5.0332	3.3581	3.4949	1.6694	1.6874×10^{-11}
270	0.89468	3.3337	5.0146	3.7341	2.6332	1.7461	1.0630×10^{-11}
300	0.75544	2.4390	5.0103	4.1072	2.0206	1.8171	5.7692×10^{-12}
330	0.67281	1.7173	5.0165	4.4799	1.5605	1.8802	1.8664×10^{-12}
360	0.62363	1.1508×10^3	5.0302	4.8555	1.2001	1.9292	-1.3041×10^{-12}
390	0.59484	728.47	5.0490	5.2381	9.1199×10^{-5}	1.9480	-3.8192×10^{-12}
420	0.57836	443.29	5.0706	5.6324	6.8869	1.9018	-5.6362×10^{-12}
450	0.56869	291.25	5.0930	6.0432	5.4646	1.7361	-6.6156×10^{-12}

Table 10. Jupiter flyby trajectories (mean distance encounter)

$T, \text{ day}$	$\int_0^T a^2 dt$ m^2/sec^3	$\dot{r}(T), \text{ m/sec}$	$h(T), \text{ m}^2/\text{sec}$	$\theta(T), \text{ rad}$	$a(0), \text{ m/sec}^2$	$\psi(0), \text{ rad}$	$\dot{a}_r(0), \text{ m/sec}^3$
180	206.81	6.1349×10^4	1.0128×10^{16}	1.8045	6.6830×10^{-3}	1.4203	5.2025×10^{-10}
240	79.523	4.4896	8.7962×10^{15}	2.1631	3.5381	1.5422	2.6454×10^{-10}
300	39.095	3.4862	8.0370	2.5036	2.1557	1.6281	1.4514×10^{-10}
360	22.757	2.8090	7.5840	2.8327	1.4417	1.6929	8.4175×10^{-11}
420	14.984	2.3207	7.3109	3.1524	1.0305	1.7435	5.0174×10^{-11}
480	10.822	1.9520	7.1513	3.4637	7.7415×10^{-4}	1.7825	2.9762×10^{-11}
540	8.3853	1.6644	7.0679	3.7674	6.0428	1.8110	1.6769×10^{-11}
600	6.8572	1.4349	7.0384	4.0649	4.8619	1.8291	8.1205×10^{-12}
660	5.8441	1.2487	7.0488	4.3580	4.0095	1.8363	2.1811×10^{-12}
720	5.1412	1.0965	7.0897	4.6494	3.3759	1.8317	-1.9668×10^{-12}
780	4.6341	9.7171×10^3	7.1553	4.9429	2.8951	1.8144	-4.8605×10^{-12}
840	4.2549	8.7046	7.2416	5.2440	2.5259	1.7827	-6.8198×10^{-12}
900	3.9612	7.3451	5.5607	5.5607	2.2438	1.7351	-8.0138×10^{-12}

Table 11. Saturn flyby trajectories (mean distance encounter)

$T, \text{ day}$	$\int_0^T a^2 dt$ m^2/sec^3	$\dot{r}(T), \text{ m/sec}$	$h(T), \text{ m}^2/\text{sec}$	$\theta(T), \text{ rad}$	$a(0), \text{ m/sec}^2$	$\psi(0), \text{ rad}$	$\dot{a}_r(0), \text{ m/sec}^3$
180	983.60	1.2323×10^5	1.6230×10^{16}	1.6255	1.4404×10^{-2}	1.4002	1.3541×10^{-9}
270	259.85	8.0465×10^4	1.2514	2.0092	6.0313×10^{-3}	1.5596	5.3084×10^{-10}
360	102.93	5.9003	1.0695	2.3584	3.2305	1.6558	2.4567×10^{-10}
450	51.860	4.6143	9.6923×10^{15}	2.6923	1.9918	1.7216	1.2664×10^{-10}
540	30.733	3.7595	9.1077	3.0161	1.3468	1.7692	6.9208×10^{-11}
630	20.464	3.1515	8.7642	3.3317	9.7238×10^{-4}	1.8033	3.8371×10^{-11}
720	14.858	2.6978	8.5727	3.6403	7.3725	1.8261	2.0442×10^{-11}
810	11.517	2.3475	8.4839	3.9435	5.8053	1.8381	9.3842×10^{-12}
900	9.3842	2.0702	8.4688	4.2436	4.7114	1.8394	2.2753×10^{-12}

Table 12. Three-dimensional optimum thrust trajectories

T , days	$\int_0^T a^2 dt$, m^2/sec^4	Terminal conditions	$a_x(0)$, m/sec^2	$a_y(0)$, m/sec^2	$a_z(0)$, m/sec^2	$\dot{a}_x(0)$, m/sec^3	$F(0)$, m^2/sec^3	$r(T)$, m	$\dot{r}(T)$, m/sec	$\alpha(T)$, deg	$\beta(T)$, deg	$h_x(T)$, m^2/sec	$h_z(T)$, m^2/sec
120	12.548	Venus circular $i(T) = 3.394$	$-1.3716 \cdot 10^{-4}$	$-1.5062 \cdot 10^{-3}$	$2.6723 \cdot 10^{-4}$	$1.5692 \cdot 10^{-10}$	-8.1451	$1.0906 \cdot 10^{11}$	1.0510	152.04	3.000	$1.0494 \cdot 10^{14}$	$3.7829 \cdot 10^{15}$
120	12.767	Venus circular $i(T) = 3.394$	$-1.3867 \cdot 10^{-4}$	$-1.5113 \cdot 10^{-3}$	$4.1807 \cdot 10^{-4}$	$1.5994 \cdot 10^{-11}$	-8.8209	$1.0806 \cdot 10^{11}$	-0.2877	152.13	1.500	$2.0103 \cdot 10^{14}$	$3.7790 \cdot 10^{15}$
120	12.959	Venus circular $i(T) = 3.394$	$-1.3908 \cdot 10^{-4}$	$-1.5097 \cdot 10^{-3}$	$4.2932 \cdot 10^{-4}$	$1.6174 \cdot 10^{-10}$	19.462	$1.0806 \cdot 10^{11}$	-0.2587	152.07	0.0046	$2.2402 \cdot 10^{14}$	$3.7778 \cdot 10^{15}$
120	13.011	Venus circular $i(T) = 3.393$	$-1.3850 \cdot 10^{-4}$	$-1.5038 \cdot 10^{-3}$	$3.5154 \cdot 10^{-4}$	$1.6156 \cdot 10^{-10}$	26.146	$1.0806 \cdot 10^{11}$	-0.1238	151.96	-1.502	$2.6089 \cdot 10^{14}$	$3.7791 \cdot 10^{15}$
120	12.804	Venus circular $i(T) = 3.395$	$-1.3699 \cdot 10^{-4}$	$-1.4978 \cdot 10^{-3}$	$1.3417 \cdot 10^{-4}$	$1.5863 \cdot 10^{-10}$	26.383	$1.0806 \cdot 10^{11}$	1.0403	151.86	-3.000	$1.0503 \cdot 10^{14}$	$3.7829 \cdot 10^{15}$
178.5	9.6590	Mars elliptical perigee encounter $i(T) = 1.864$	$7.3417 \cdot 10^{-4}$	$1.1648 \cdot 10^{-3}$	$-1.4513 \cdot 10^{-4}$	$-2.0370 \cdot 10^{-11}$	2.9176	$2.064 \cdot 10^{11}$	-0.0613	139.72	-1.780	$-5.2962 \cdot 10^{13}$	$5.4692 \cdot 10^{15}$
165	39.652	Mercury $r = 5.11 \cdot 10^7$ $i = 7.003$	$-3.0890 \cdot 10^{-3}$	$-1.9168 \cdot 10^{-3}$	$-1.5756 \cdot 10^{-4}$	$3.0434 \cdot 10^{-11}$	-24.559	$6.3813 \cdot 10^{10}$	$7.7701 \cdot 10^3$	307.22	6.4950	$1.2398 \cdot 10^{13}$	$2.7058 \cdot 10^{15}$
165	39.868	Mercury $r = 5$ $i = 7.004$	$-1.0597 \cdot 10^{-3}$	$-1.6137 \cdot 10^{-3}$	$6.9388 \cdot 10^{-4}$	$1.2248 \cdot 10^{-10}$	17.082	$5.7832 \cdot 10^{10}$	$-9.9018 \cdot 10^3$	285.70	6.6920	$-9.7859 \cdot 10^{13}$	$2.7069 \cdot 10^{15}$
165	30.940	Mercury apogee encounter $i = 7.004$	$-9.4460 \cdot 10^{-4}$	$-2.0638 \cdot 10^{-3}$	$-7.3745 \cdot 10^{-4}$	$8.2687 \cdot 10^{-11}$	-29.050	$6.9794 \cdot 10^{10}$	-0.0037	375.77	-3.387	$2.8944 \cdot 10^{14}$	$2.6931 \cdot 10^{15}$

Table 13. Equatorial radii and orbital velocities of orbits of various altitudes

Planet	R, km	Orbital Velocity, km/sec			
		200 miles	500 miles	1000 miles	2000 miles
Mercury	2420	2.81	2.67	2.31	1.96
Venus	6200	7.05	6.80	6.44	5.87
Earth	6378	7.70	7.40	7.08	6.44
Mars	3400	3.39	3.19	2.92	2.54
Jupiter	71,400	42.1	41.9	41.7	41.2
Saturn	60,400	25.0	24.9	24.7	24.4
Uranus	23,800	15.5	15.3	15.1	14.6
Neptune	22,300	17.4	17.2	16.9	16.4
Pluto	7200:	6.64:	6.44:	6.14:	5.54:

**Table 14. Weight percentage comparison for chemical and advanced systems
(Jupiter 570-day flight)**

Mission	Chemical propulsion system	Advanced propulsion system	
	Final vehicle weight, %	Final vehicle weight, %	Final vehicle weight minus powerplant, %
Flyby	17	79	54
Orbiter	8%	63	38

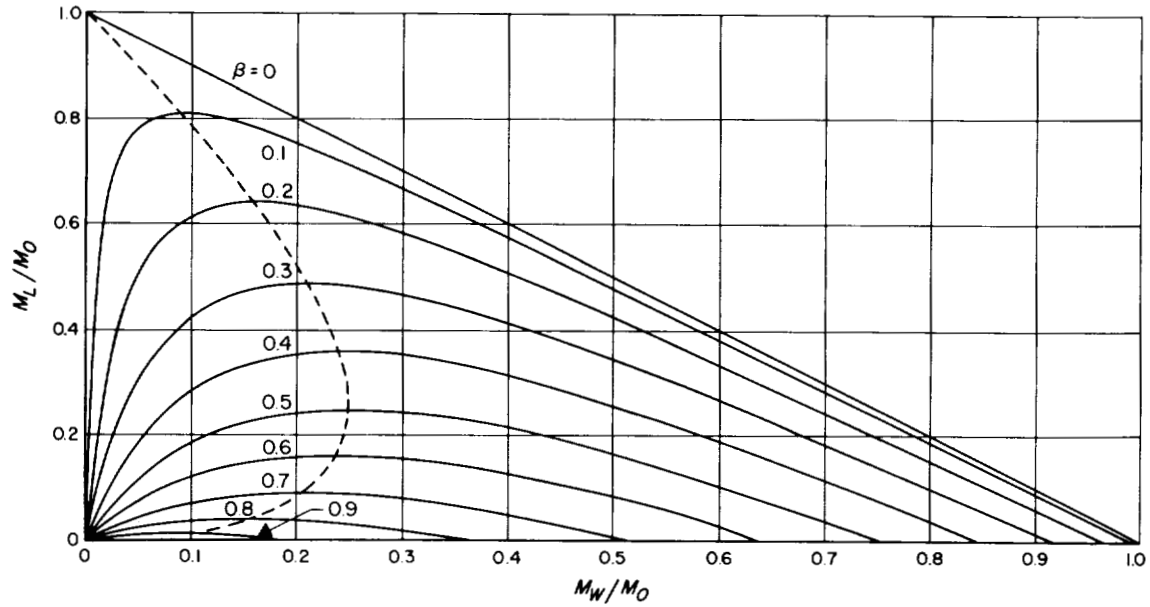


Fig. 1. Payload on structures mass ratio vs powerplant mass ratio

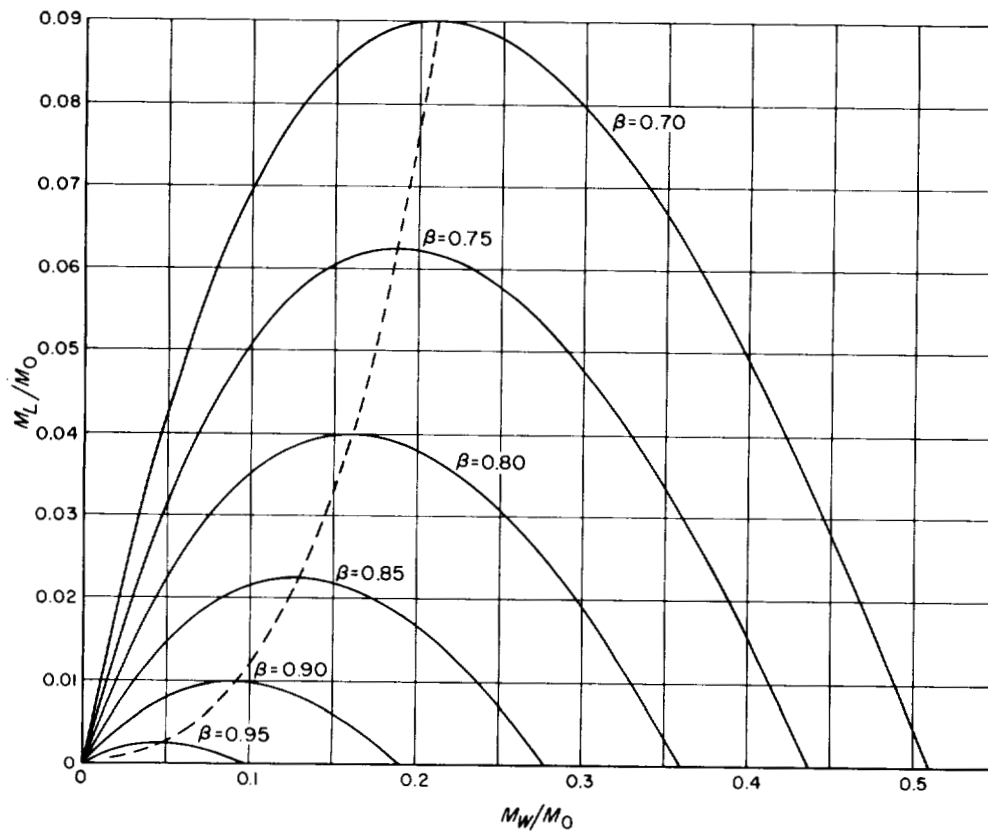


Fig. 2. Payload on structures mass ratio vs powerplant mass ratio

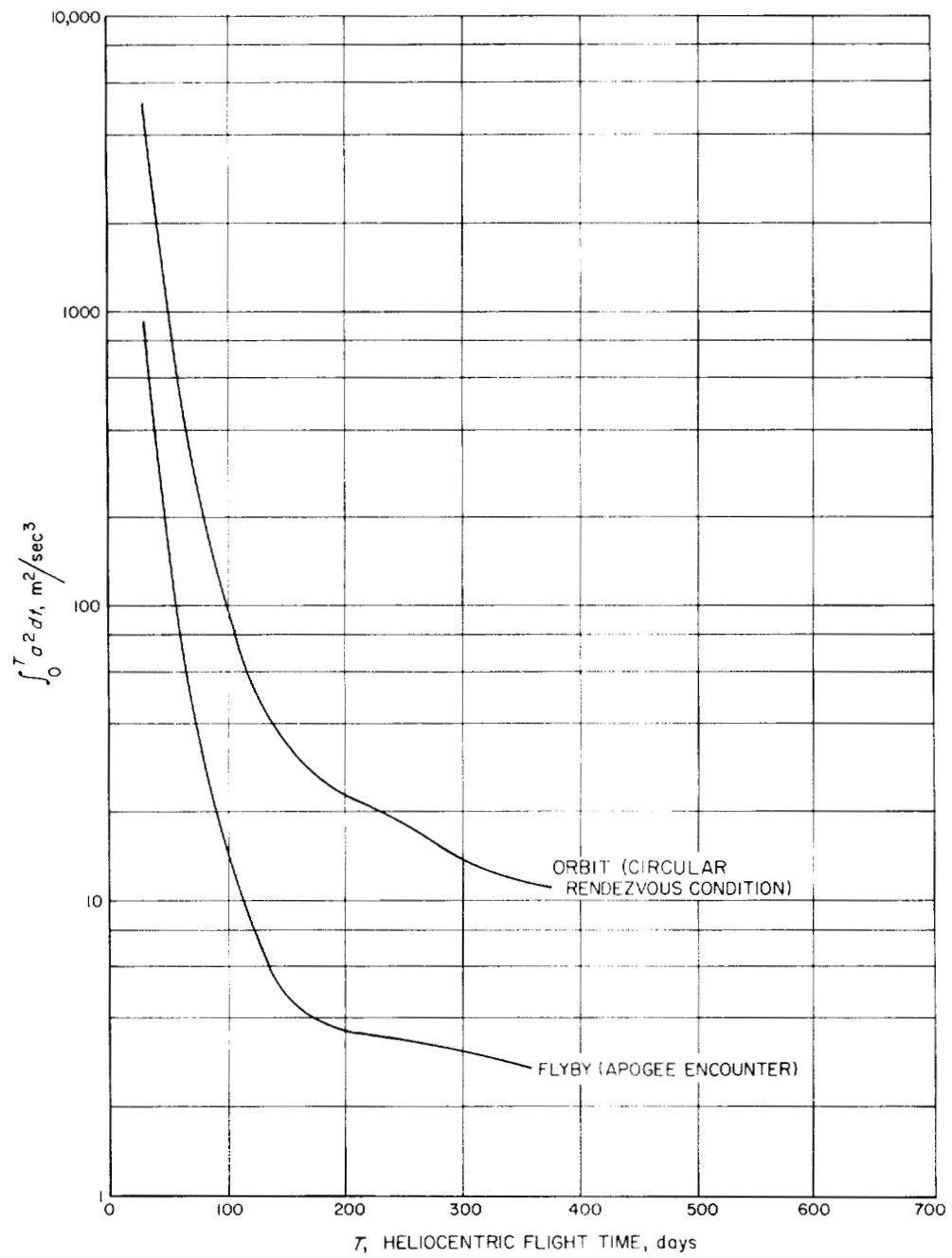


Fig. 3. Payload capabilities: Mercury trajectories

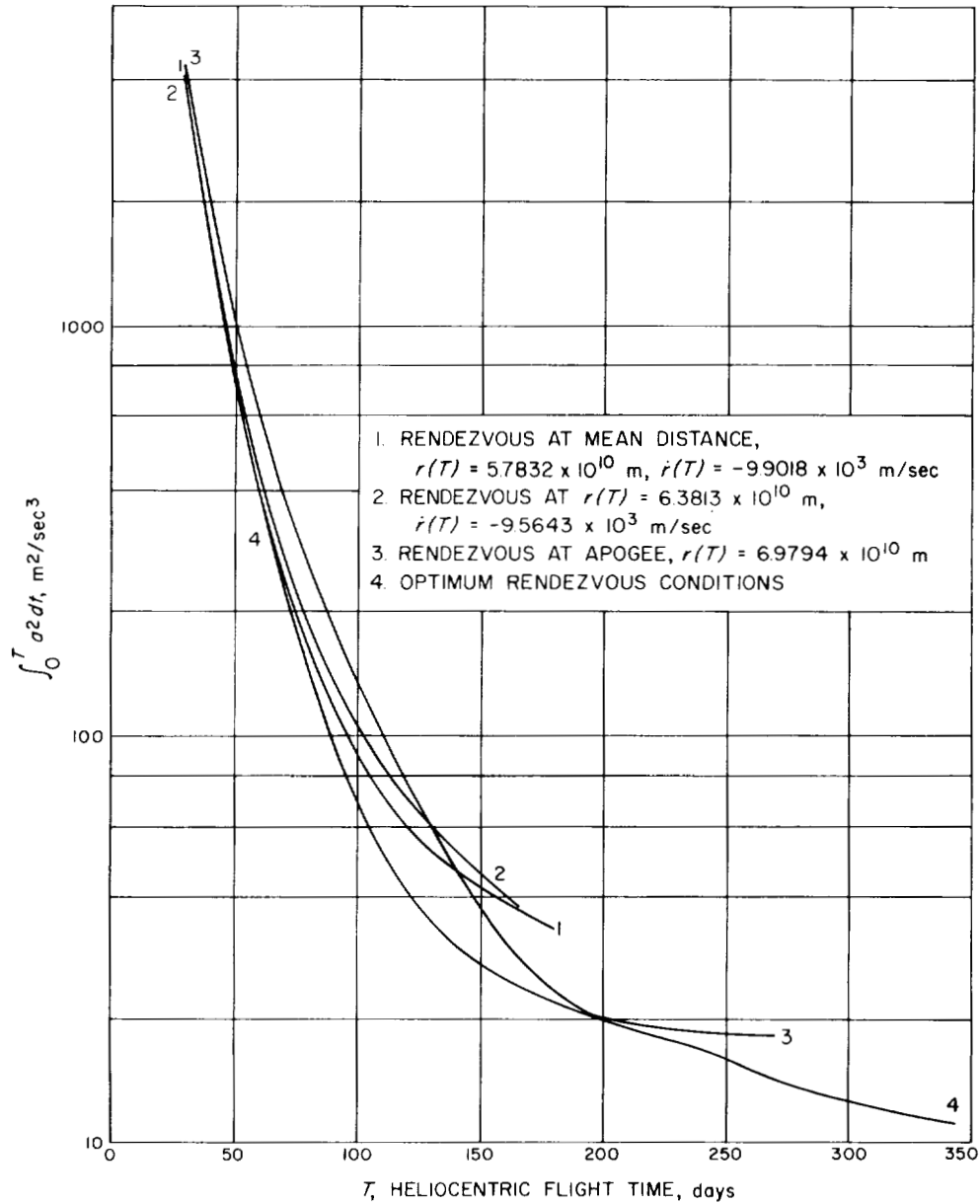


Fig. 4. Payload capabilities: Mercury orbiter trajectories

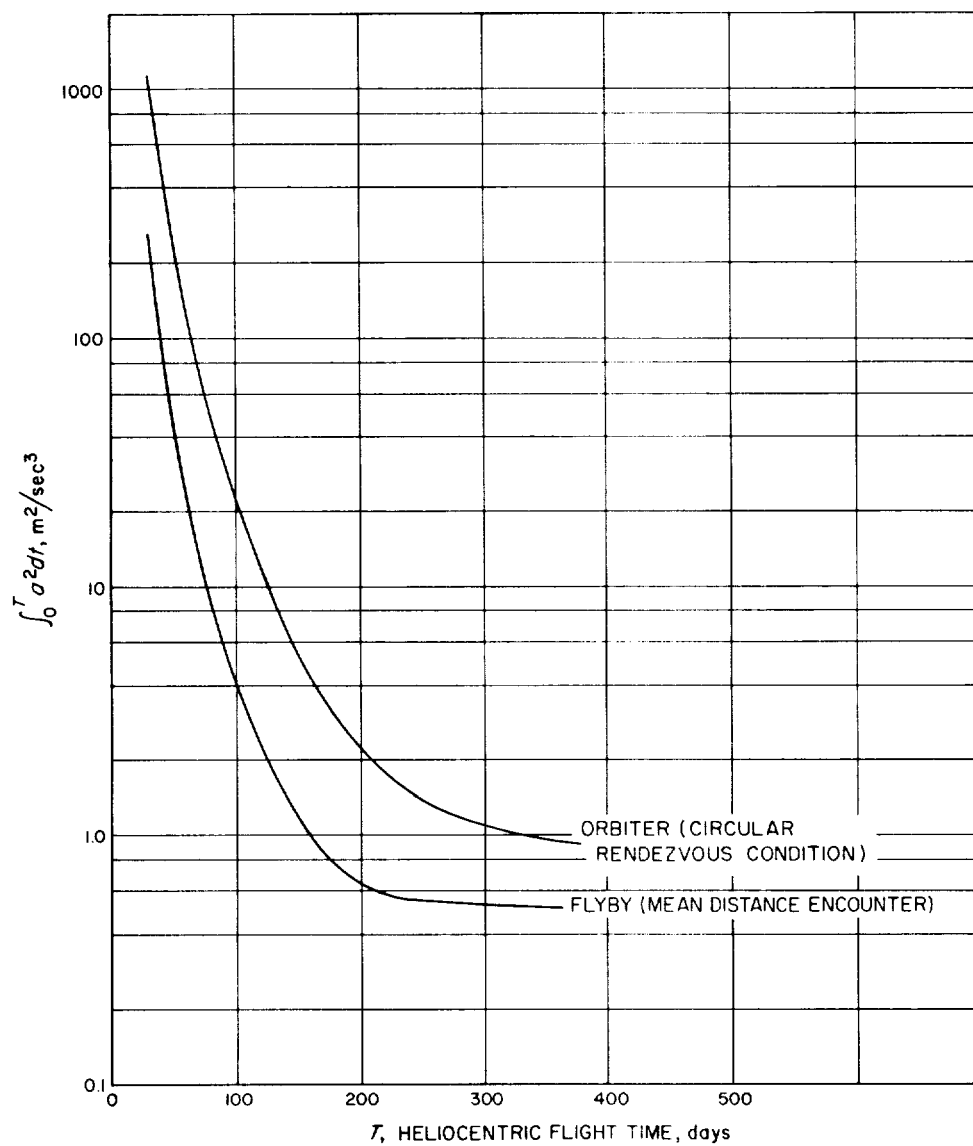


Fig. 5. Payload capabilities: Venus trajectories

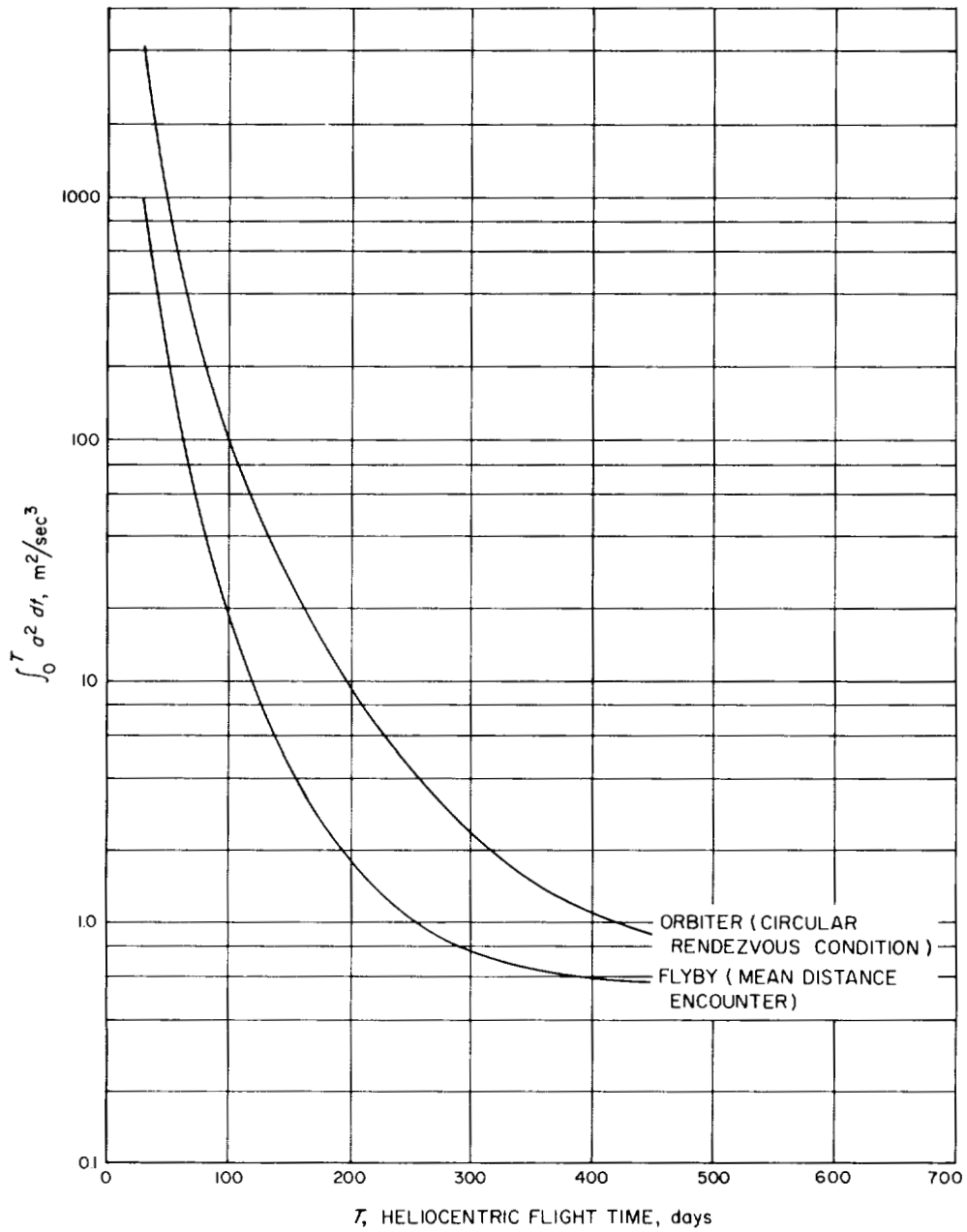


Fig. 6. Payload capabilities: Mars trajectories

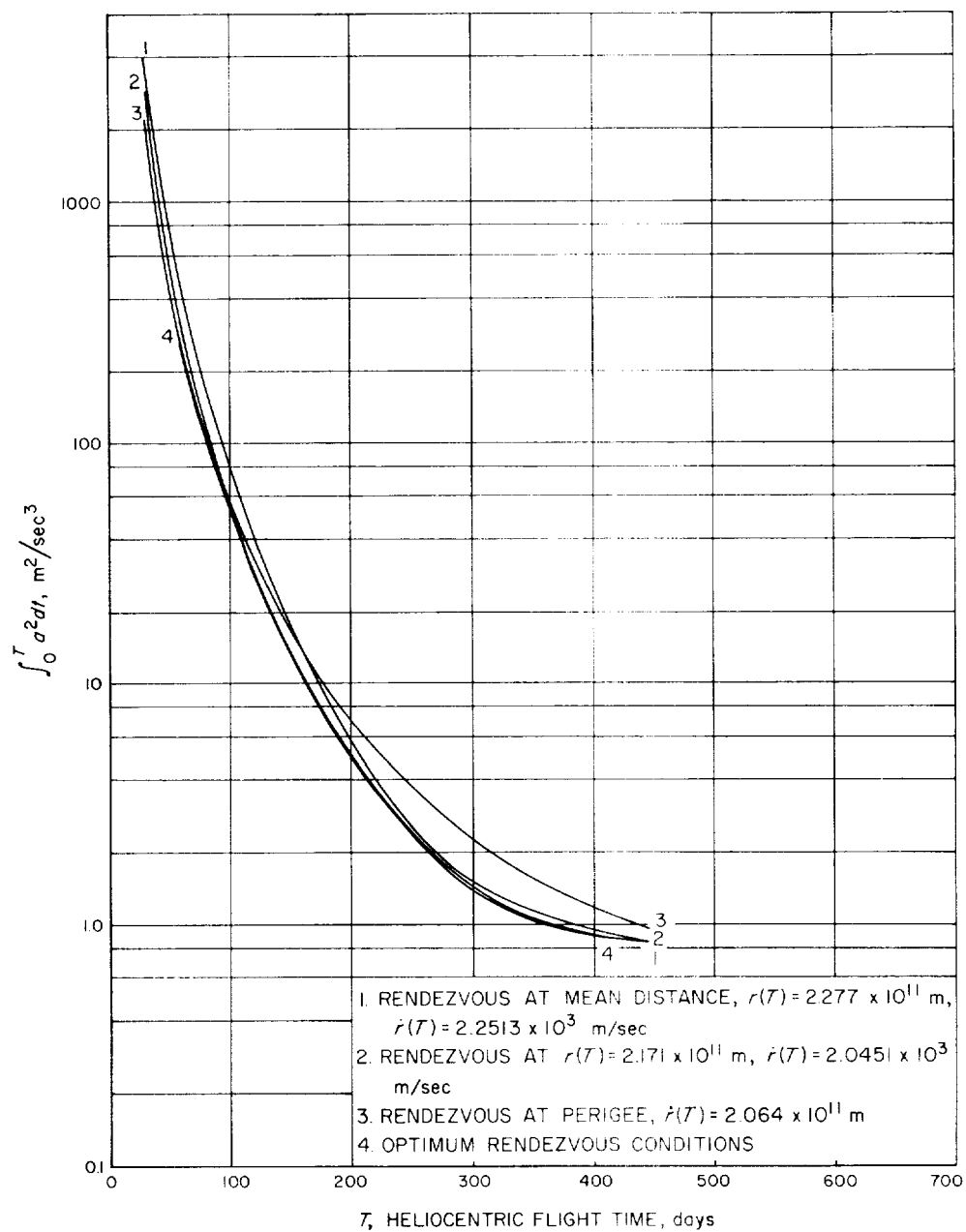


Fig. 7. Payload capabilities: Mars orbiter trajectories

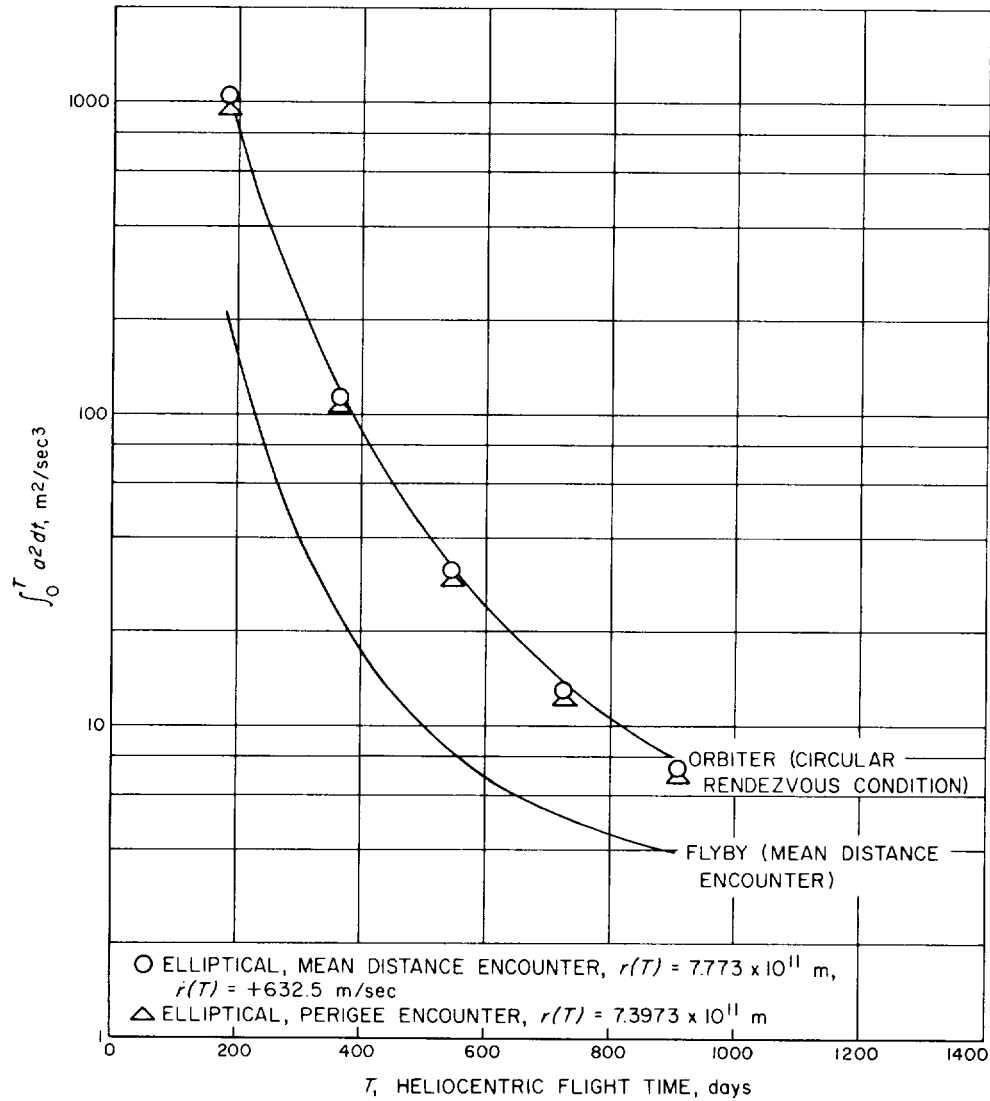


Fig. 8. Payload capabilities: Jupiter trajectories

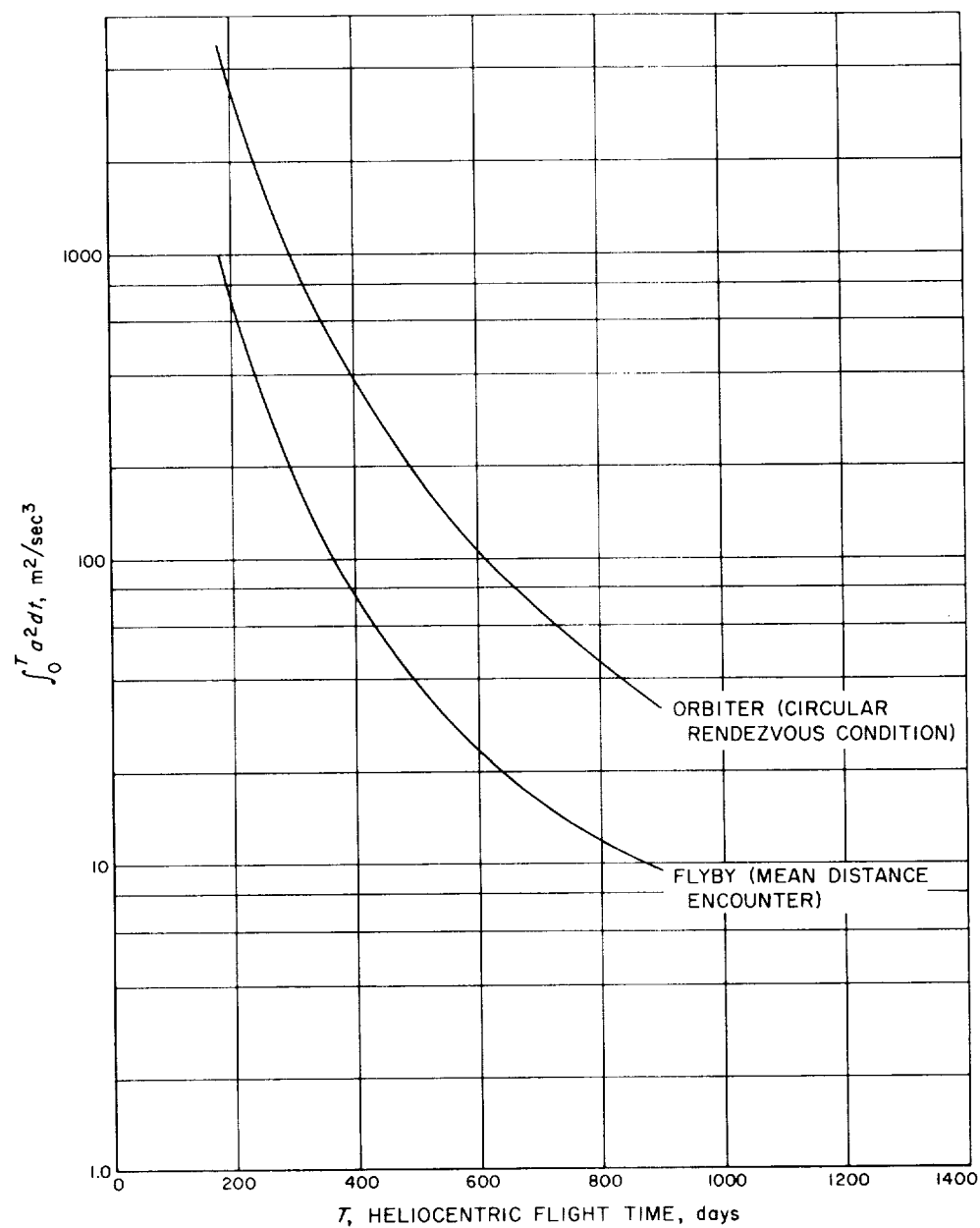


Fig. 9. Payload capabilities: Saturn trajectories

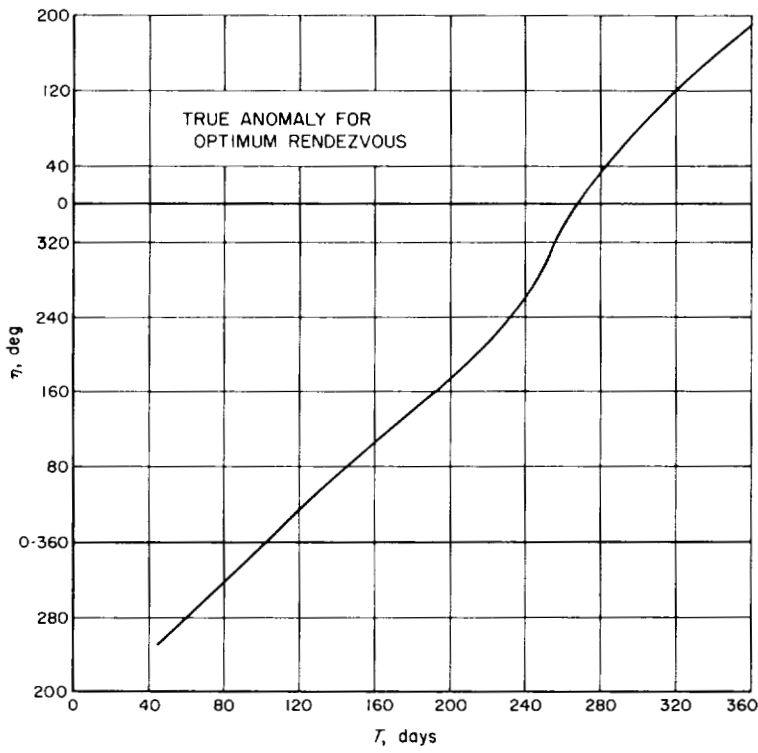


Fig. 10. Mercury orbiter trajectories

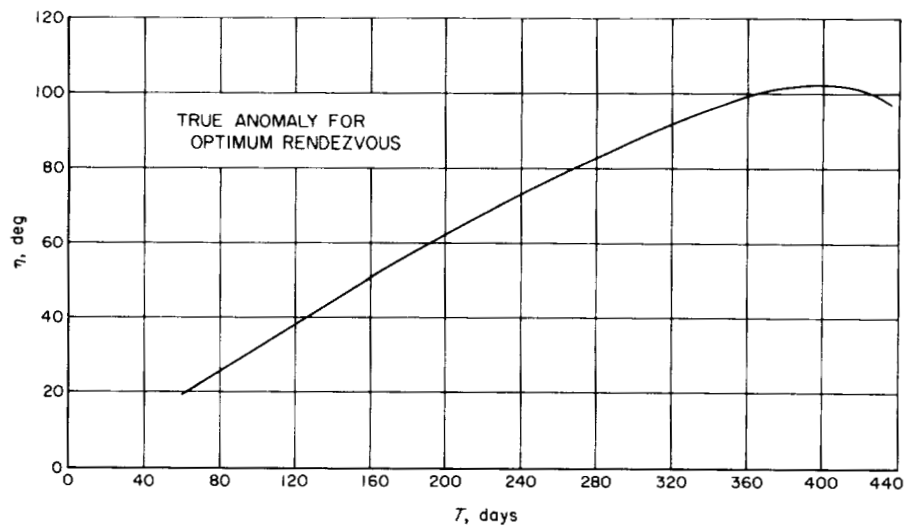


Fig. 11. Mars orbiter trajectories

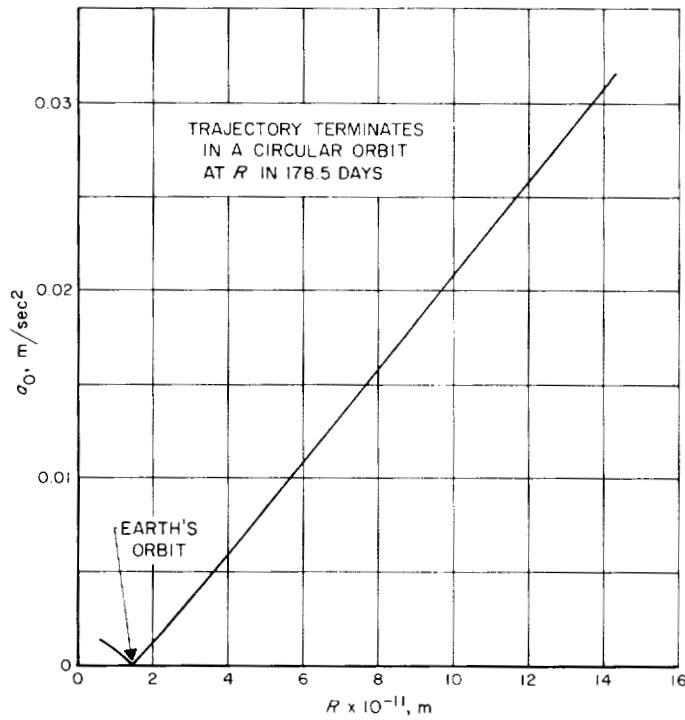
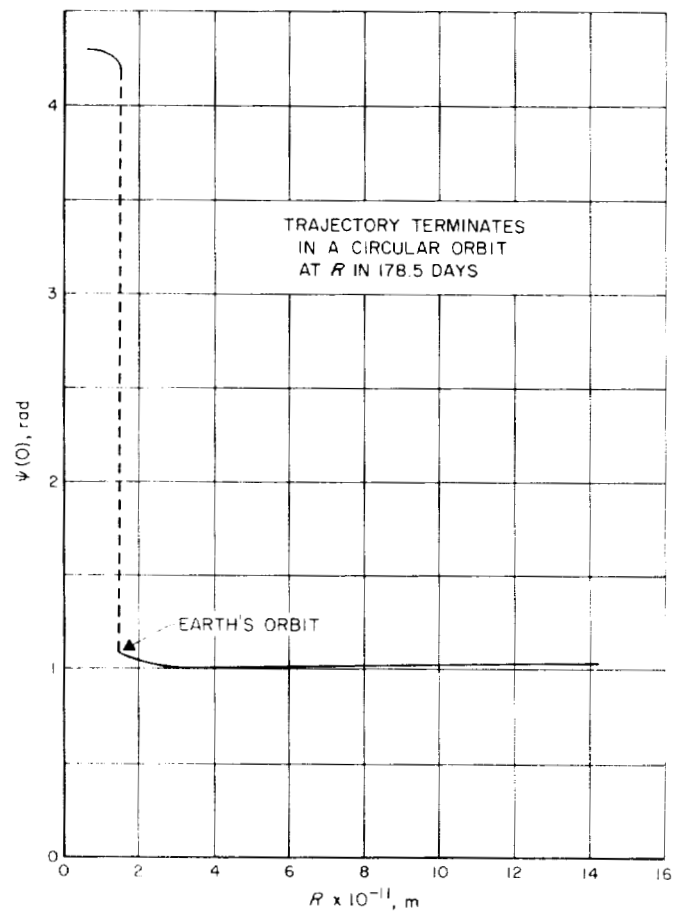


Fig. 12. Power-limited optimum thrust program:
initial thrust acceleration

Fig. 13. Power-limited optimum thrust program:
initial thrust angle



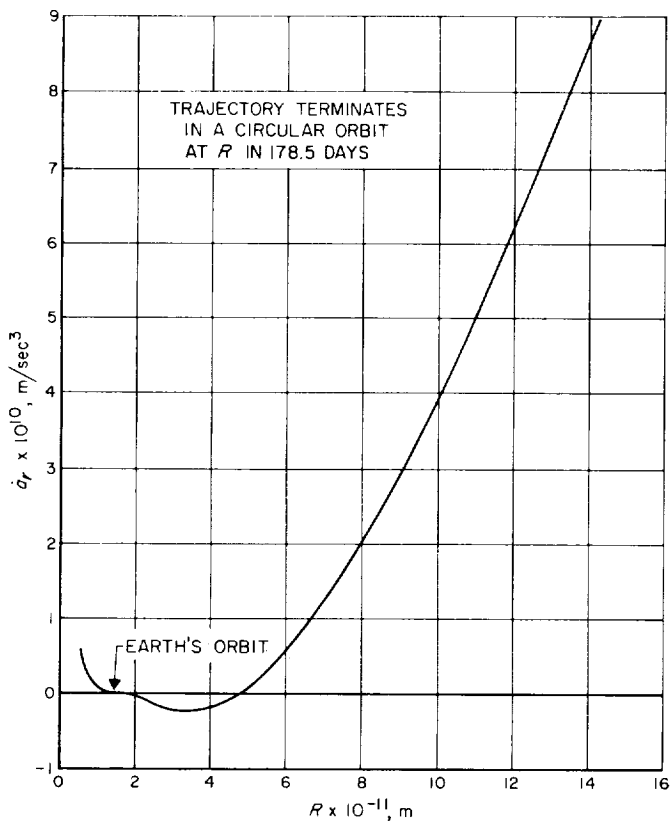


Fig. 14. Power-limited optimum thrust program:
initial time derivative of the
radial thrust acceleration

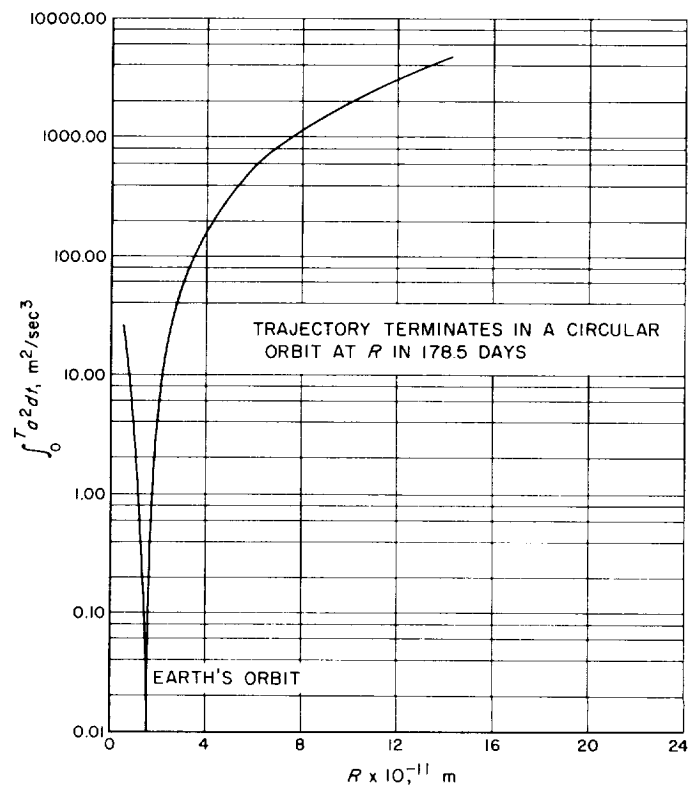


Fig. 15. Power-limited optimum thrust program

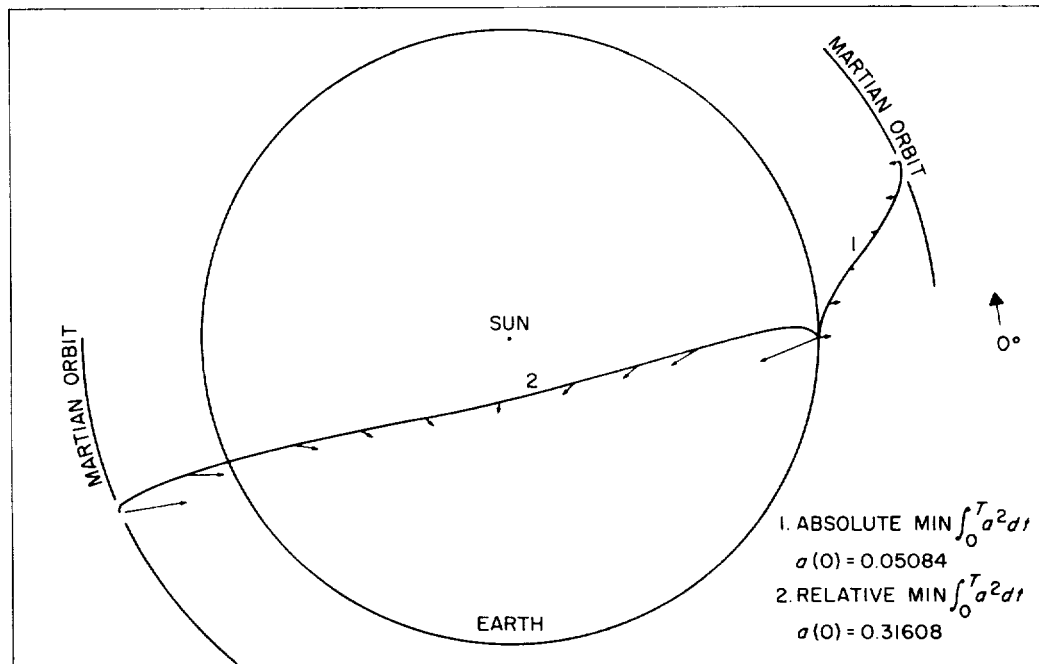


Fig. 16. Mars orbiting trajectories, 30-day heliocentric flight time, two-dimensional optimum thrust program for power-limited propulsion

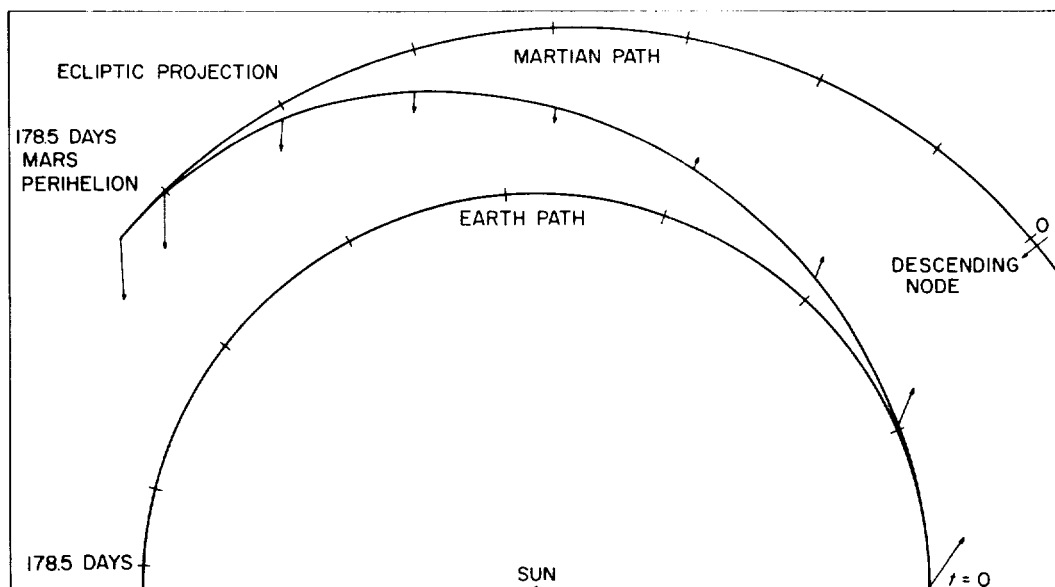


Fig. 17. Mars orbiting trajectories, 178-day heliocentric flight time, three-dimensional optimum thrust program for power-limited propulsion

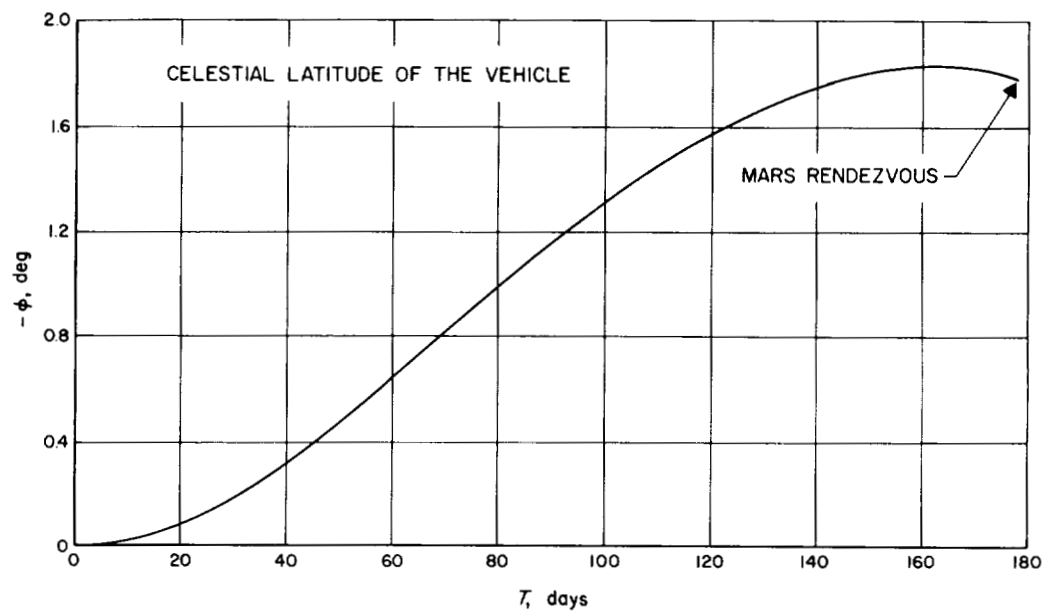


Fig. 18. Mars orbiting trajectories, 178-day heliocentric flight time, three-dimensional optimum thrust program for power-limited propulsion

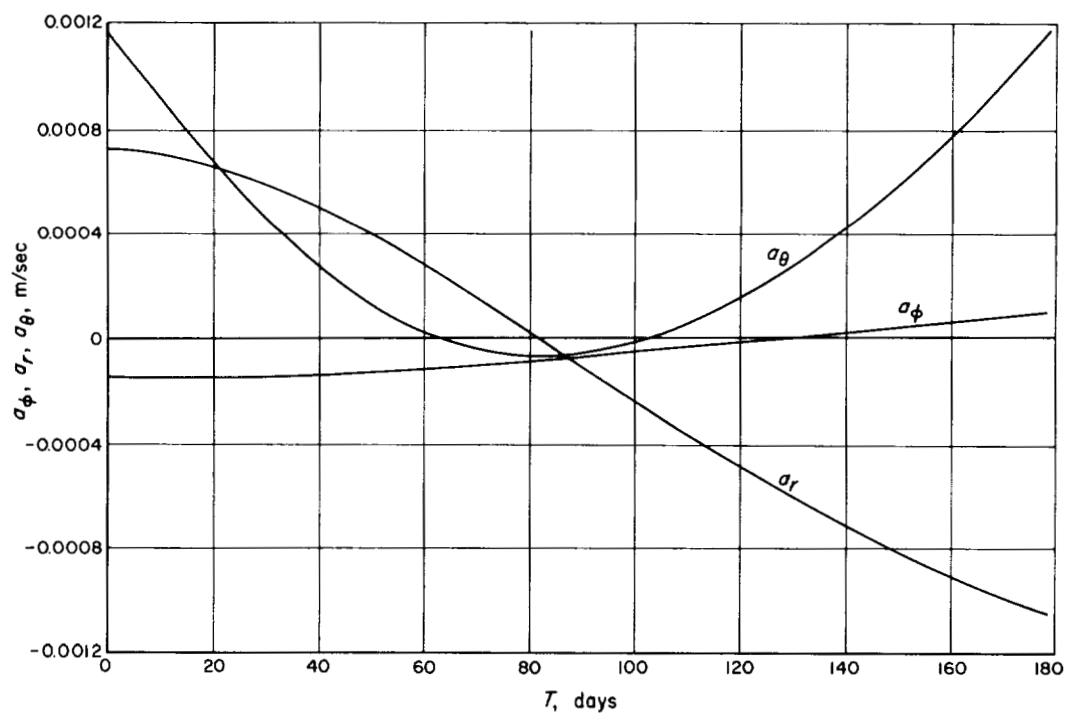


Fig. 19. Mars orbiting trajectories, 178-day heliocentric flight time, three-dimensional optimum thrust program for power-limited propulsion

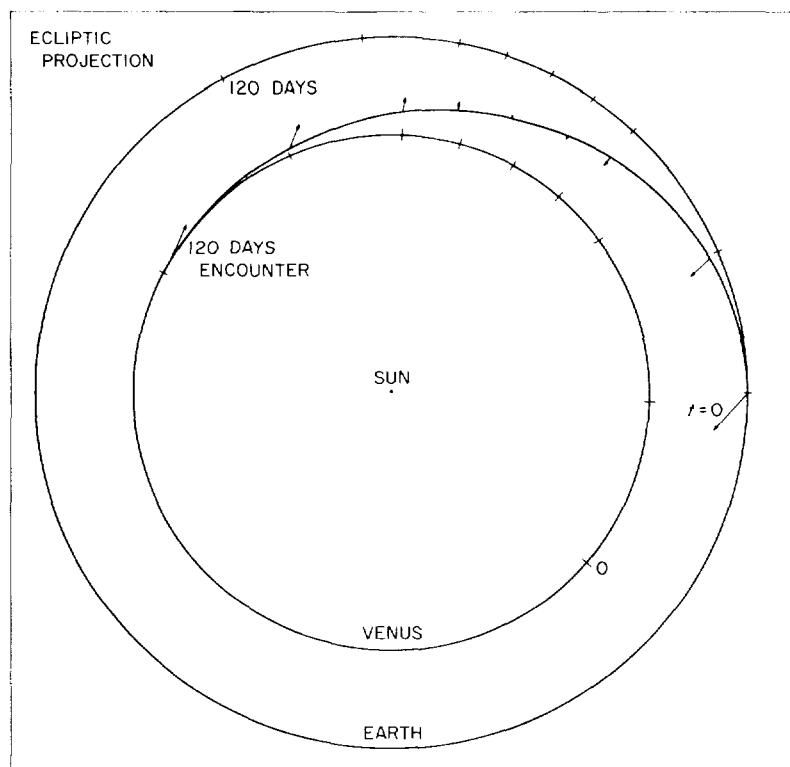


Fig. 20. Venus orbiting trajectories, 120-day heliocentric flight time, three-dimensional optimum thrust program for power-limited propulsion

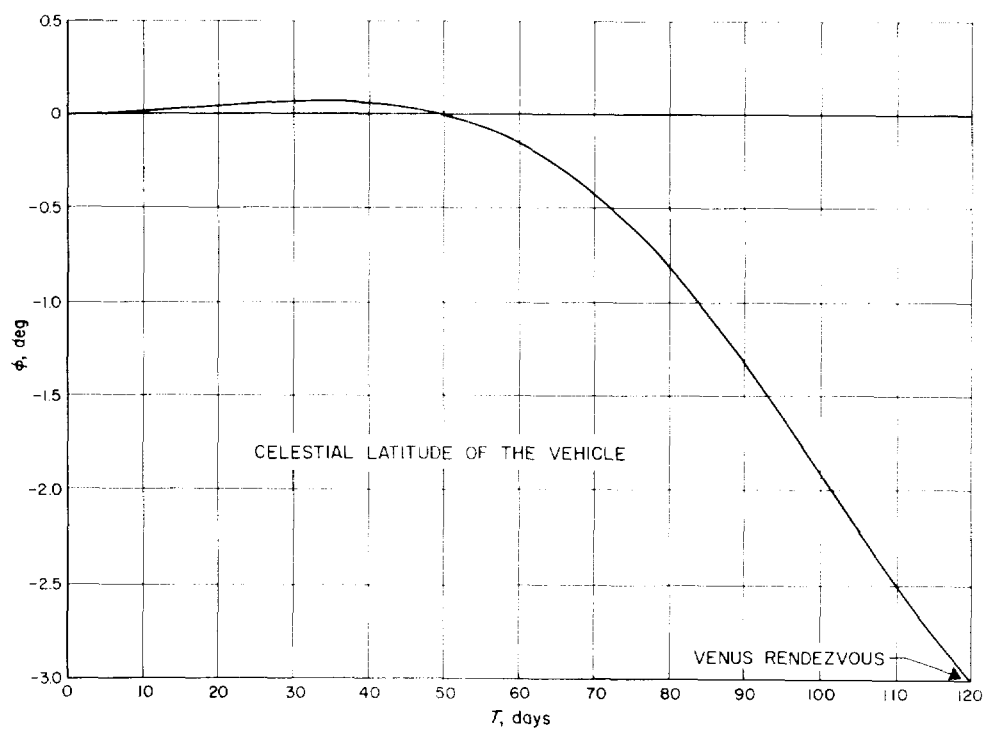


Fig. 21. Venus orbiting trajectories, 120-day heliocentric flight time, two-dimensional optimum thrust program for power-limited propulsion

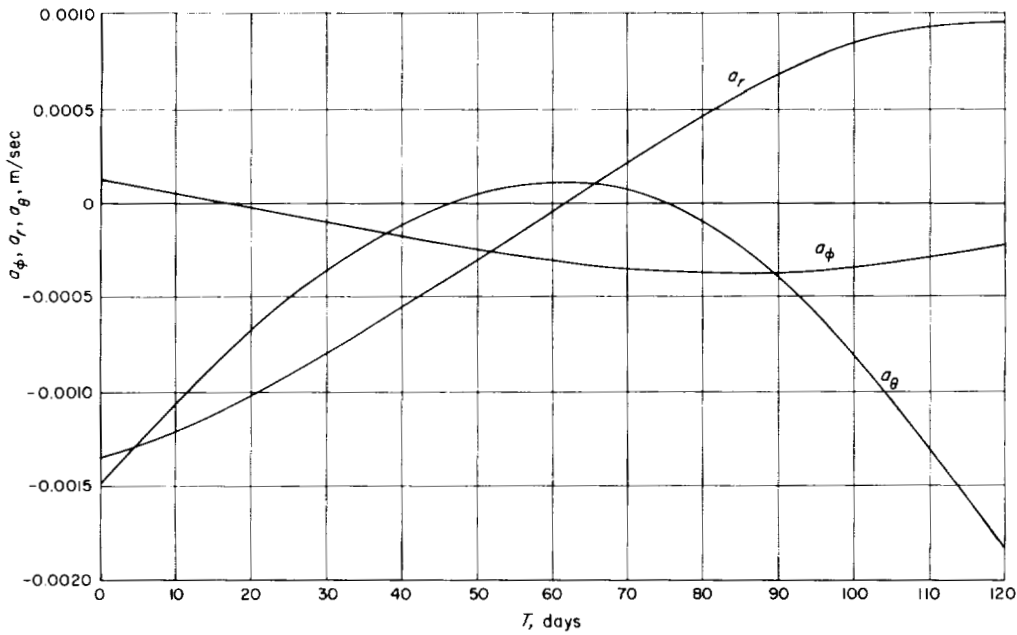
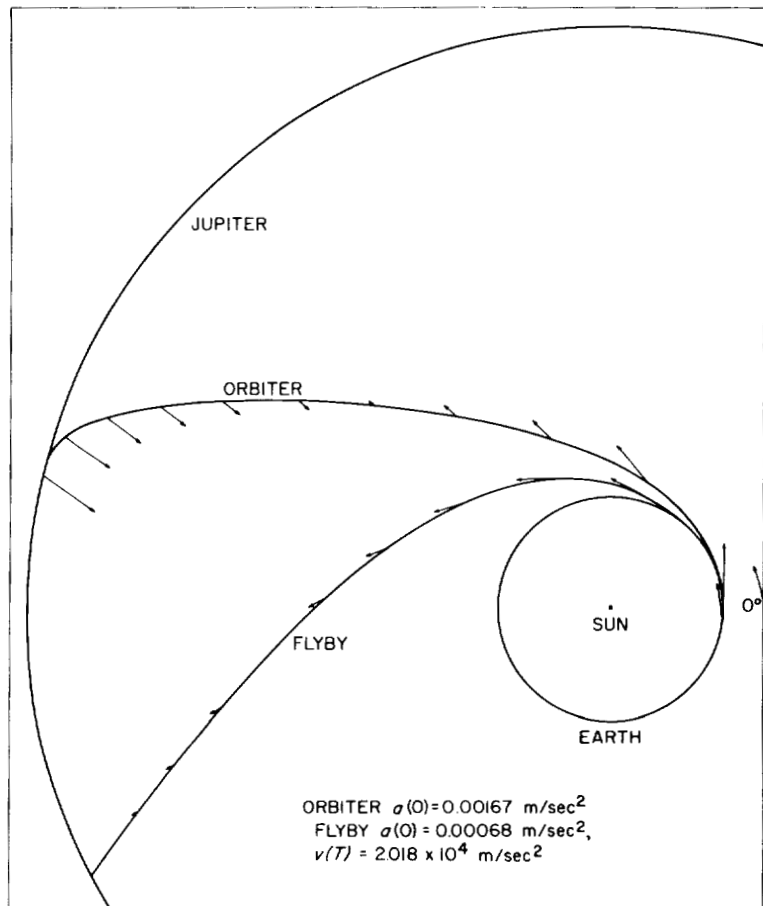


Fig. 22. Venus orbiting trajectories, 120-day heliocentric flight time, three-dimensional optimum thrust program for power-limited propulsion

Fig. 23. Jupiter orbiting trajectories, 510-day heliocentric flight time, two-dimensional optimum thrust program for power-limited propulsion



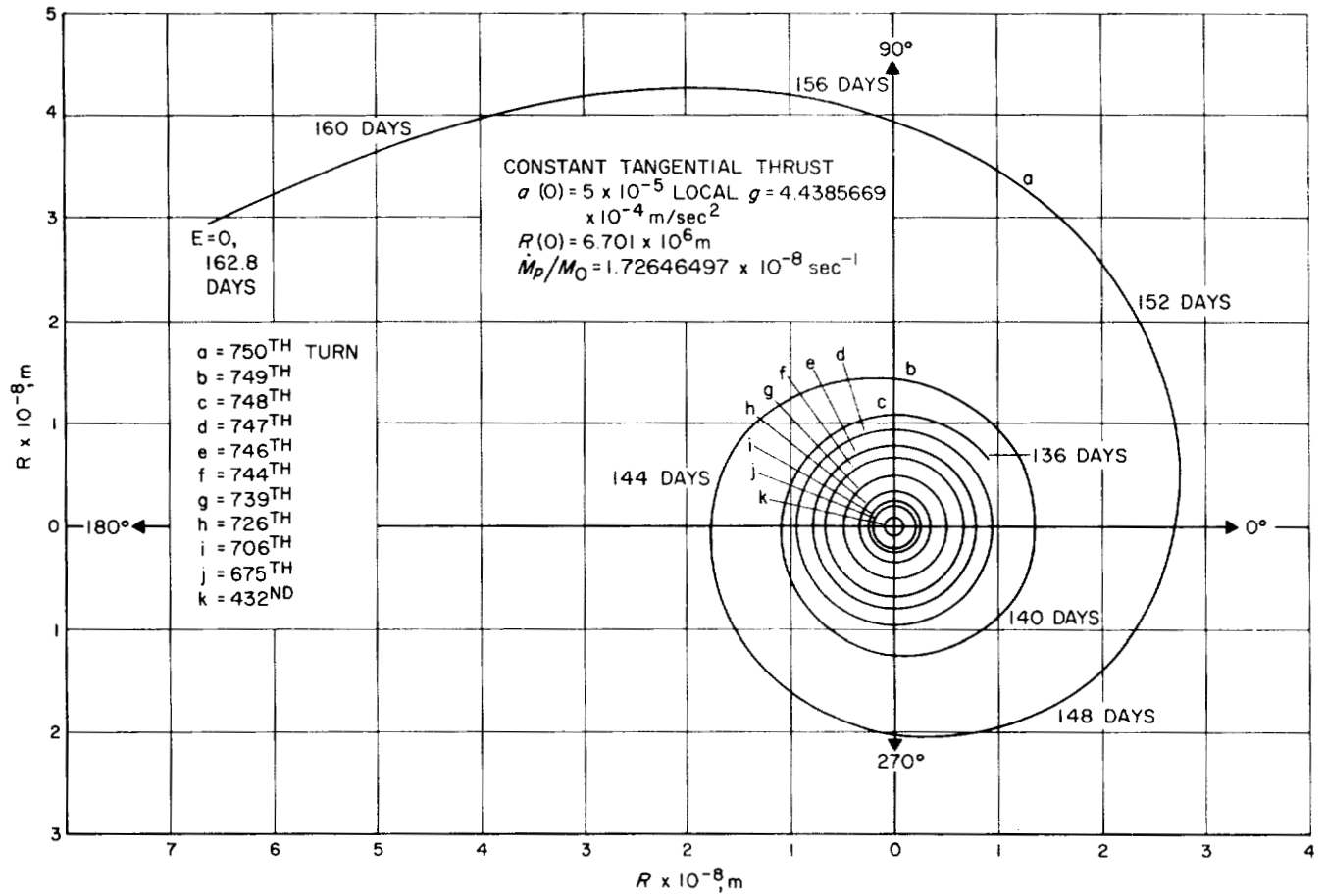


Fig. 24. Earth-centered low thrust trajectory

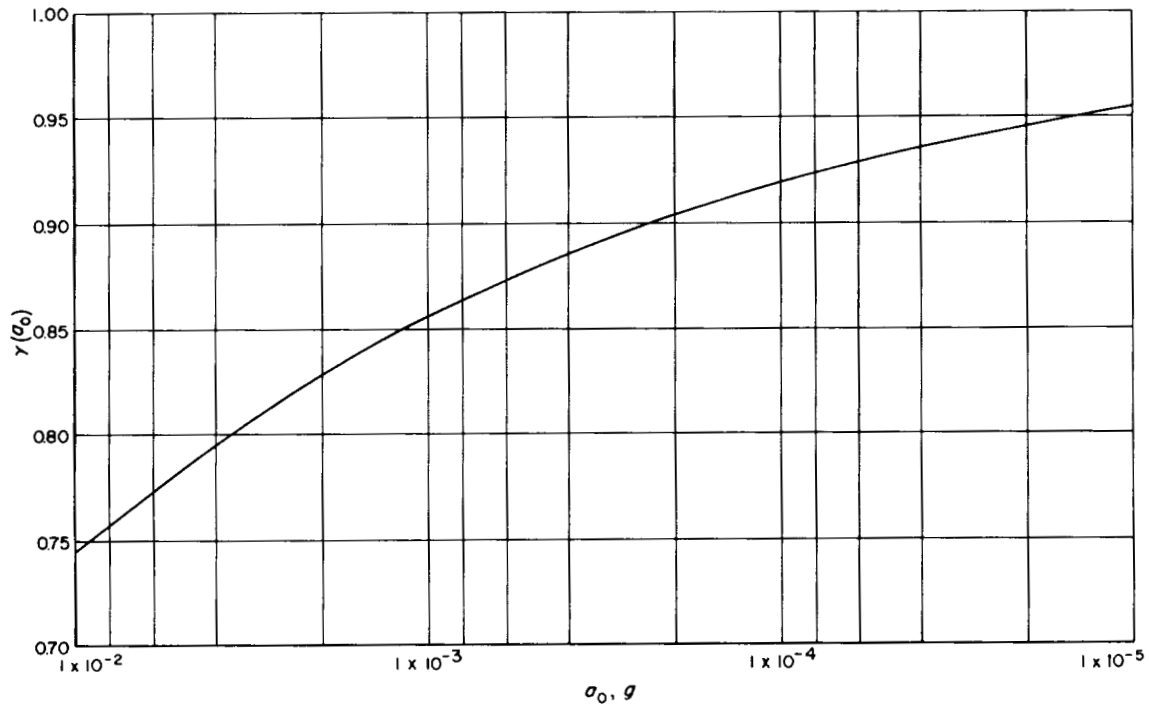


Fig. 25. Correction factor for constant tangential thrust

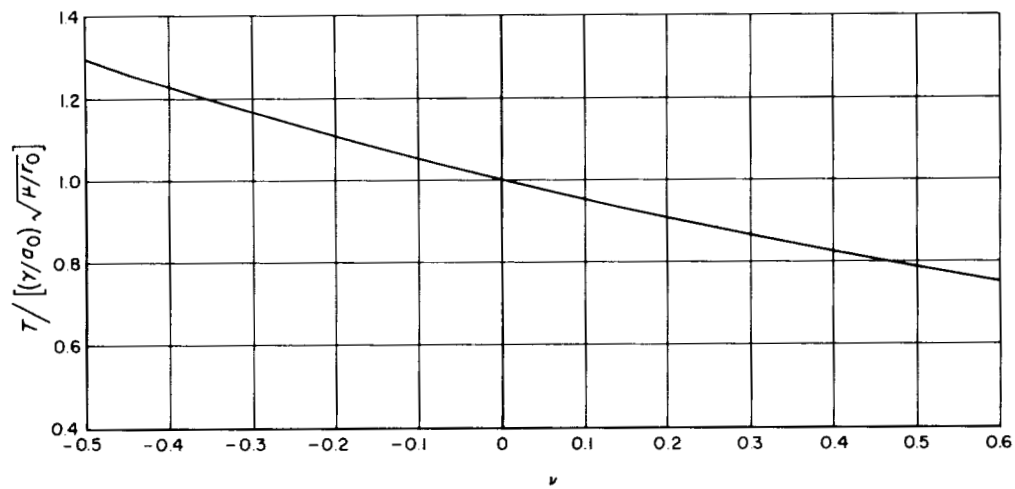


Fig. 26. Variation of escape time with vehicle mass loss

Appendix A. Analytical Basis of Thrust Program

In this appendix, the origin of the necessary conditions that

$$\int_0^T a^2 dt = \text{minimum}$$

and the accompanying terminal conditions are considered in detail. This is a calculus of variations problem in which the above integral is minimized subject to certain constraining equations and boundary conditions. Considered here is that class of problems where boundary conditions are applied only at the initial and terminal points and where all the variables of the problem are continuously differentiable. An Euler-Lagrange formulation of this variational problem will be employed.

In general terms, the integral to be minimized is defined as

$$I = \int_0^T Q[X_1(t), \dots, X_n(t), \dot{X}_1(t), \dots, \dot{X}_n(t), t] dt \quad (\text{A-1})$$

where the X_i 's are the state variables of the system (e.g., phase space coordinates, accelerations, etc.), the \dot{X}_i 's are their time derivatives, and T is a fixed time. The constraining equations will be expressed as

$$G_j(X_1, \dots, X_n, \dot{X}_1, \dots, \dot{X}_n, t) = 0, j = 1, 2, \dots, r < n \quad (\text{A-2})$$

There may be as many as $2n$ boundary conditions in this problem. These may be specified values of the state variables themselves, or specified values of functions of these variables. In either case, these conditions may be written in functional form as

$$H_l(X_1, \dots, X_n, t) \big|_{t=0} = 0, l = 1, 2, \dots, n \quad (\text{A-3})$$

$$H_l(X_1, \dots, X_n, t) \big|_{t=T} = 0, l = n+1, n+2, \dots, 2n$$

where it is understood that some of these functions may be identically zero if not all $2n$ of the boundary conditions are specified.

We wish to obtain the functional forms of the $X_i(t)$'s such that I is a minimum subject to the conditions in Eq. (A-2) and (A-3). It may be shown that the necessary and sufficient conditions that I take on a stationary value is given by the following Euler-Lagrange equations and their subsidiary end conditions:

$$\frac{\partial Q}{\partial X_i} + \sum_{j=1}^r \lambda_j \frac{\partial G_j}{\partial X_i} - \frac{d}{dt} \left[\frac{\partial Q}{\partial \dot{X}_i} + \sum_{j=1}^r \lambda_j \frac{\partial G_j}{\partial \dot{X}_i} \right] = 0, \quad i = 1, 2, \dots, n \quad (\text{A-4})$$

$$\left[\frac{\partial Q}{\partial \dot{X}_i} + \sum_{j=1}^r \lambda_j \frac{\partial G_j}{\partial \dot{X}_i} + \sum_{l=1}^n \kappa_l \frac{\partial H_l}{\partial \dot{X}_i} \right] \bigg|_{t=0} \delta X_i(0) = 0, \quad i = 1, 2, \dots, n \quad (\text{A-5})$$

and

$$\left[\frac{\partial Q}{\partial \dot{X}_i} + \sum_{j=1}^r \lambda_j \frac{\partial G_j}{\partial \dot{X}_i} + \sum_{l=n+1}^{2n} \kappa_l \frac{\partial H_l}{\partial \dot{X}_i} \right] \bigg|_{t=T} \delta X_i(T) = 0, \quad i = 1, 2, \dots, n \quad (\text{A-6})$$

where the $\lambda_j(t)$'s and κ_l 's are Lagrange multipliers.

The quantities $\delta X_i(0)$ and $\delta X_i(T)$ are the variations of X_i at the end points. If the value of a particular X_i is specified at an end point, then δX_i is zero at that end point and the corresponding κ_l (κ_i , if initial point, κ_{n+i} , if terminal point) is zero. If X_i is not specified, the coefficient of δX_i is zero and the corresponding H_i may be identically zero or a function of the state variables.

Equations (A-2) and (A-4) serve to define the $n + r$ variables of time, $X_i(t)$ and $\lambda_j(t)$. Equations (A-3), (A-5), and (A-6) define the $2n$ κ_l 's and the $2n$ independent constants of motion which result from the solution of Eq. (A-2) and (A-4).

This formulation is now applied to the case at hand using Cartesian coordinates (x_1, x_2, x_3) . A vehicle is considered traveling in a conservative force field under thrust acceleration. The origin of the coordinate system is inertial. Thus, the state variables are

$$X_i = x_i \quad i = 1, 2, 3 \quad (\text{A-7})$$

$$X_{i+3} = v_i \quad i = 1, 2, 3 \quad (\text{A-8})$$

$$X_{i+6} = a_i \quad i = 1, 2, 3 \quad (\text{A-9})$$

where v_i is the velocity component and a_i is the thrust acceleration component. The integrand of I is

$$Q = a^2 = \sum_{i=1}^3 a_i^2 \quad (\text{A-10})$$

and the constraining equations are Newton's laws of motion which are

$$\dot{v}_i + \frac{\partial V}{\partial x_i} - a_i = 0 = G_i \quad i = 1, 2, 3 \quad (\text{A-11})$$

$$v_i - \dot{x}_i = 0 = G_i + 3 \quad i = 1, 2, 3$$

where V is the potential of the force field. Upon applying Eq. (A-4) and eliminating the 6 Lagrange multipliers the Euler equations become

$$\ddot{a}_i + \sum_{j=1}^3 a_j \frac{\partial^2 V}{\partial x_i \partial x_j} = 0 \quad i = 1, 2, 3 \quad (\text{A-12})$$

Both Eq. (A-11) and (A-12) may be written in vector form; thus one finds the necessary conditions that I be minimized are

$$\ddot{\mathbf{a}} + (\mathbf{a} \cdot \nabla) \nabla V = 0 \quad (\text{A-13})$$

and

$$\ddot{\mathbf{r}} + \nabla V - \mathbf{a} = 0 \quad (\text{A-14})$$

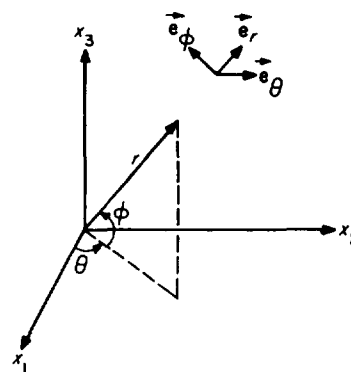
where \mathbf{r} is the position vector.

Equations (A-13) and (A-14) form a twelfth-order system, and twelve constants of integration are needed to completely specify the thrust program and the trajectory. These are provided by Eq. (A-3), (A-5), and (A-6). For a two-dimensional formulation of this problem the number reduces to eight. One quite valuable constant of integration can be provided from analysis. By combining Eq. (A-13) and (A-14) in a dot product and integrating over time it may be shown that

$$\dot{\mathbf{a}} \cdot \dot{\mathbf{r}} - \frac{1}{2} \dot{\mathbf{a}}^2 + \mathbf{a} \cdot \nabla V = C \quad (\text{A-15})$$

which is recognized as the first integral of the Euler-Lagrange equations. Equations (A-13) and (A-14) are quite general and apply to a vehicle in any conservative force field. They apply also when the field is time-varying, but Eq. (A-15) is modified.

These results are now applied to a two-body inverse-square force field employing spherical coordinates to benefit from the spherical symmetry of this problem. This coordinate system and the direction of the basic vectors are illustrated in the accompanying sketch. The state variables for this formulation are r , θ , ϕ , u , h_θ , h_ϕ , a_r , a_θ , and a_ϕ , where u is radial velocity and h_θ and h_ϕ are the components of angular momentum. After some manipulation it may be shown that Eq. (A-13) and (A-14) become



$$\ddot{a}_r + \frac{3a_r}{r^4} \left[h^2 - \frac{2\mu r}{3} \right] - \frac{1}{r} [a_\theta^2 + a_\phi^2] - \frac{2h_\phi \tan \phi}{r^4} (\mathbf{h} \cdot \mathbf{a}) - \frac{h_\theta F(t)}{r^3} - \frac{K_1 h_\phi}{r^3 \cos \phi} = 0 \quad (\text{A-16})$$

$$F(t) + 2r^2 \frac{d}{dt} \left[\frac{a_\phi}{r} \right] - \frac{4h_\theta a_r}{r} + \frac{2h_\phi a_\theta \tan \phi}{r} = 0 \quad (\text{A-17})$$

$$\dot{F}(t) - \frac{2h_\phi}{r^3 \cos^2 \phi} (\mathbf{h} \cdot \mathbf{a}) - \frac{K_1 h_\phi \sin \phi}{r^2 \cos^2 \phi} = 0 \quad (\text{A-18})$$

$$r^2 \frac{d}{dt} \left[\frac{a_\theta}{r} \right] + \frac{h_\phi}{r} (2a_r - a_\phi \tan \phi) - \frac{\tan \phi}{r} (\mathbf{h} \cdot \mathbf{a}) - \frac{K_1}{2 \cos \phi} = 0 \quad (\text{A-19})$$

$$\dot{u} - \frac{h^2}{r^3} + \frac{\mu}{r^2} - a_r = 0 = G_1 \quad (\text{A-20})$$

$$u - \dot{r} = 0 = G_2 \quad (\text{A-21})$$

$$\dot{h}_\theta - \frac{h_\phi^2 \tan \phi}{r^2} + r a_\phi = 0 = G_3 \quad (\text{A-22})$$

$$\dot{h}_\phi + \frac{h_\theta h_\phi \tan \phi}{r^2} - r a_\theta = 0 = G_4 \quad (\text{A-23})$$

$$h_\theta + r^2 \dot{\phi} = 0 = G_5 \quad (\text{A-24})$$

$$h_\phi - r^2 \dot{\theta} \cos \phi = 0 = G_6 \quad (\text{A-25})$$

$$h^2 = h_\phi^2 + h_\theta^2 \quad (\text{A-26})$$

where h is the angular momentum per unit mass of the vehicle and μ is the gravitational constant of the central body. The quantity $F(t)$ is an auxiliary variable, essentially one of the Lagrange multipliers which could not be easily eliminated. The quantity K_1 is a constant of integration resulting from the cyclical nature of the variable θ . Equation (A-15) becomes

$$a^2 - 2\dot{a}_r \dot{r} + \frac{2a_r}{r^3} [h^2 - \mu r] - \frac{K_1 h_\phi}{r^2 \cos \phi} - \frac{h_\theta F(t)}{r^2} - \frac{2h_\phi \tan \phi}{r^3} (h \cdot a) = K_2 \quad (\text{A-27})$$

The quantities K_1 and K_2 are the only constants of motion which have been found. Equation (A-27) is useful in checking the accuracy of the numerical integrations of Eq. (A-16)–(A-25). For the two-dimensional formulation these equations reduce to the set obtained in Ref. 1, which are

$$\ddot{a}_r - \frac{a_r}{r^4} (2\mu r - 3h^2) - \frac{a_\theta^2}{r} - \frac{K_1 h}{r^3} = 0 \quad (\text{A-28})$$

$$r^2 \frac{d}{dt} \left(\frac{a_\theta}{r} \right) + \frac{2h a_r}{r} - \frac{K_1 h}{2} = 0 \quad (\text{A-29})$$

$$\dot{u} - \frac{h^2}{r^3} + \frac{\mu}{r^2} - a_r = 0 = G_1 \quad (\text{A-30})$$

$$u - \dot{r} = 0 = G_2 \quad (\text{A-31})$$

$$\dot{h} - r a_\theta = 0 = G_3 \quad (\text{A-32})$$

$$h - r^2 \dot{\theta} = 0 = G_4 \quad (\text{A-33})$$

and

$$a^2 - 2\dot{a}_r \dot{r} + \frac{2a_r}{r^3} (h^2 - \mu r) - \frac{K_1 h}{r^2} = K_2 \quad (\text{A-34})$$

Both sets of equations, Eq. (A-16)–(A-25) and Eq. (A-28)–(A-34), have been programmed for numerical solution and are discussed in the text. Equations (A-28)–(A-34) have been coupled with a search routine (described in the text) to obtain trajectories which satisfy the appropriate terminal conditions.

Terminal Conditions

In practice, the state variables X_i are nearly always all specified at the initial point of the trajectory and, in fact, most of them usually have specified terminal values. For those cases where the X_i 's are specified, the corresponding H_l 's have the particularly simple form

$$H_i = X_i - X_{i_{\text{specified}}} = 0 \quad (\text{A-35})$$

Furthermore, the corresponding κ_i 's in Eq. (A-5) and (A-6) are zero. There are some functions of the state variables such as energy, inclination, etc., which might be specified terminally.

For example, suppose that in the inverse-square force field case the terminal energy, momentum, and the component of angular momentum normal to the plane $\phi = 0$ are specified. The remainder of the state variables are unspecified terminally, and all the state variables are specified initially. For this case, Eq. (A-3) becomes

$$\left. \begin{aligned} H_l &= X_l(0) - X_{l_{\text{specified}}}(0) = 0 & l &= 1, 2, \dots, n \\ H_{n+1} &= \left[E_{\text{specified}} - \frac{1}{2} \left(u^2 + \frac{h^2}{r^2} \right) + \frac{\mu}{r} \right] \bigg|_{t=T} = 0 \\ H_{n+2} &= \left[h_{\text{specified}}^2 - h_\phi^2 - h_\theta^2 \right] \bigg|_{t=T} = 0 \\ H_{n+3} &= \left[h_{z_{\text{specified}}} - h_\phi \cos \phi \right] \bigg|_{t=T} = 0 \\ H_l &\equiv 0, & l &= n+4, \dots, 2n \end{aligned} \right\} \quad (\text{A-36})$$

It may be shown that the terminal or transversality expressions to be satisfied as given by Eq. (A-6) become for this case

$$\dot{a}_r(T) \dot{r}(T) + \frac{a_r(T)}{r^3(T)} [\mu r(T) - h^2(T)] = 0 \quad (\text{A-37})$$

$$2h_\phi(T) [a(T) \cdot h(T)] \tan \phi(T) + r(T) h_\theta(T) F(T) = 0 \quad (\text{A-38})$$

and

$$K_1 = 0 \quad (\text{A-39})$$

Incorporating these conditions in Eq. (A-27) reveals that

$$K_2 = a^2(T) \quad (\text{A-40})$$

Quite generally, commencing from a circular orbit yields

$$K_2 = a^2(0) \quad (\text{A-41})$$

For two dimensions, Eq. (A-37), (A-39), and (A-40) hold. The orbiter trajectories in Tables 2 and 4, which intercept the orbits of Mercury and Mars, optimally were obtained by satisfying Eq. (A-37) and the specified values of energy and angular momentum of these two planets.

If, instead, only the energy is specified, it may be shown that the transversality expressions are given by Eq. (A-37) and

$$\frac{a_r(T)}{\dot{r}(T)} = \frac{a_\theta(T)}{h_\phi(T)/r(T)} = \frac{a_\phi(T)}{-h_\theta/r(T)} \quad (\text{A-42})$$

That is, the thrust acceleration vector is along the terminal velocity vector. Additional conditions for this case are

$$F(T) = 0 \quad (\text{A-43})$$

$$K_1 = 0 \quad (\text{A-44})$$

Further, since Eq. (A-42) implies that $h(T) \cdot a(T)$ is zero, it follows that Eq. (A-40) holds for this case also.

Consider now the three-dimensional flyby mission commencing from specified initial conditions with only the position coordinates $r(T)$, $\theta(T)$, and $\phi(T)$ being specified terminally. For this case it may be shown that

$$a_r(T) = a_\theta(T) = a_\phi(T) = 0 \quad (\text{A-45})$$

must be satisfied in order to minimize $\int_0^T a^2 dt$. These three conditions along with the three specified terminal position coordinates and the six initial conditions make up the twelve quantities required for evaluating the twelve constants of integration of Eq. (A-16)–(A-25). If only the terminal value of r is specified, then, in addition to Eq. (A-45), one obtains

$$F(T) = K_1 = 0 \quad (\text{A-46})$$

from which it follows that

$$K_2 = -2\dot{a}_r(T) \dot{r}(T) \quad (\text{A-47})$$

This case is quite important and applies also to the two-dimensional problem. The two-dimensional flyby missions described in the text have K_1 taken as zero and use as terminal conditions:

$$\left. \begin{aligned} r(T) &= r(T)_{\text{specified}} \\ a_r(T) &= 0 \\ a_\theta(T) &= 0 \end{aligned} \right\} \quad (\text{A-48})$$

The search routine mentioned earlier finds for a particular mission the values of $a_r(0)$, $\dot{a}_r(0)$, and $a_\theta(0)$ which satisfy the expressions in Eq. (A-48).

The two-dimensional orbiter mission type described in the text specifies the terminal values of $\dot{r}(T)$, $r(T)$, and $h(T)$. The exceptions to this for Mercury and Mars have been discussed. The only terminal expression applicable in this case is $K_1 = 0$. This is more restrictive than specifying angular momentum and energy only, since an additional constraint is specified, namely, the position or true anomaly on the orbit at which rendezvous occurs. Equation (A-37) does not, in general, hold for this case. Only for circular orbits do these specifications coincide. The orientation of the terminal ellipse relative to the initial point of the trajectory is not specified in either case since $K_1 = 0$.

One-Dimensional Example

Consider a vehicle travelling in a field-free region in one dimension which is at rest initially and reaches a specified distance L in a flight time T . Consider two mission types: (1) at $t = T$ the vehicle is at rest; (2) at $t = T$ the velocity is not specified. These are the one-dimensional analogues of the orbiter and flyby missions. Equations (A-13), (A-14), and (A-15) reduce to

$$\left. \begin{aligned} \ddot{a} &= 0 \\ \ddot{X} - a &= 0 \\ \dot{a}\dot{X} - \frac{1}{2}a^2 &= C = -\frac{1}{2}a^2(0) = -\frac{1}{2}a^2(T), \text{ orbiter} \\ \dot{a}\dot{X} - \frac{1}{2}a^2 &= C = -\frac{1}{2}a^2(0) = \dot{a}(T)\dot{X}(T), \text{ flyby} \end{aligned} \right\} \quad (\text{A-49})$$

a fourth-order system.

For the orbiter mission the solutions to these equations satisfying the boundary conditions are

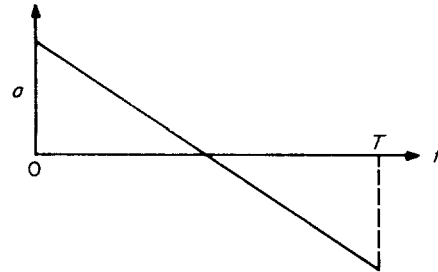
$$a = \frac{6L}{T^2} \left(1 - \frac{2t}{T} \right) \quad (\text{A-50})$$

$$X = L \left(\frac{t}{T} \right)^2 \left(3 - \frac{2t}{T} \right) \quad (\text{A-51})$$

Thus, a is antisymmetric about $t = (T/2)$.

It follows that

$$\int_0^T a^2 dt = \frac{12 L^2}{T^3}$$

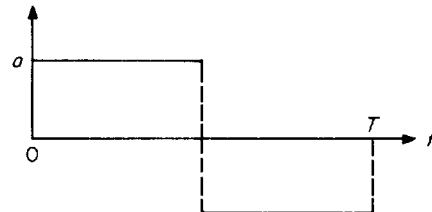


(A-52)

This is the best thrust program that can be employed and satisfy the mission requirements. Now, suppose that an alternate thrust program is employed—one of constant thrust acceleration but which may be positive or negative. To satisfy the mission, one accelerates to the midpoint in time, then decelerates at the same level.

It is easily shown that the required thrust acceleration is

$$|a| = \frac{4L}{T^2}$$



(A-53)

from which it follows that

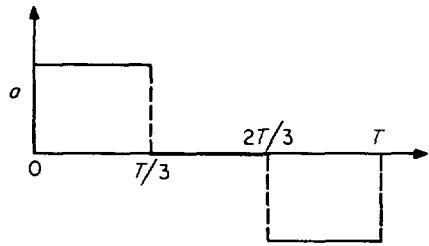
$$\int_0^T a^2 dt = \frac{16 L^2}{T^3} = \frac{4}{3} \text{ optimum value} \quad (\text{A-54})$$

By placing a coast period from $T/3 \leq t \leq 2T/3$, it may be shown that one obtains the optimum performance capable with a constant thrust acceleration program. For this case

$$|a| = \frac{9}{2} \frac{L}{T^2} \quad (\text{A-55})$$

for which there results

$$\int_0^T a^2 dt = \frac{27}{2} \frac{L^2}{T^2} = \frac{9}{8} \text{ optimum value} \quad (\text{A-56})$$



These examples, although trivial, do lend insight into the more complicated problems of interplanetary trajectories. The dependency of $\int_0^T a^2 dt$ on L^2/T^3 is a basic behavior and may be seen in Fig. 3-9. The use of constant thrust programs with coast periods in interplanetary trajectories does, in the few cases studied, degrade $\int_0^T a^2 dt$ by at least 10%.

For the flyby mission, the solution to Eq. (A-49), without involving the C expression in Eq. (A-49), is

$$\left. \begin{aligned} a &= \alpha T \left(\frac{t}{T} - \frac{1}{3} \right) + \frac{2L}{T^2} \\ X &= \frac{1}{6} \alpha T^3 \left[\left(\frac{t}{T} \right)^3 - \left(\frac{t}{T} \right)^2 \right] + L \left(\frac{t}{T} \right)^2 \end{aligned} \right\} \quad (\text{A-57})$$

where α is an undetermined constant of integration. By evaluating $\int_0^T a^2 dt$ and differentiating with respect to α ,

one finds that $\int_0^T a^2 dt$ is a minimum when

$$\alpha = - \frac{3L}{T^3} \quad (\text{A-58})$$

which is, of course, also obtained from the relation

$$C = - \frac{1}{2} a^2(0) = \dot{a}(T) \dot{X}(T)$$

With this value of α , Eq. (A-57) becomes

$$\left. \begin{aligned} a &= \frac{3L}{T^2} \left(1 - \frac{t}{T} \right) \\ X &= \frac{1}{2} L \left(\frac{t}{T} \right)^2 \left(3 - \frac{t}{T} \right) \end{aligned} \right\} \quad (\text{A-59})$$

from which there results

$$\int_0^T a^2 dt = \frac{3L^2}{T^3} \quad (\text{A-60})$$

Thus, the flyby requires $1/4$ the $\int_0^T a^2 dt$ of the orbiter mission. Figures 3, 5, 6, 8, and 9 show, for interplanetary trajectories, that this factor varies from about $1/5$ to about $1/2$. The initial acceleration level is $1/2$ orbiter value, which is also roughly the case in interplanetary trajectories.

Appendix B. Origin and Utilization of Expressions Describing Planetocentric Portions of Interplanetary Trajectories

This appendix presents a derivation of the semiempirical formulas, applicable to planetocentric trajectories, which describe the spiral motion of a vehicle about the planet. These expressions are very accurate when the thrust to local weight ratio of the vehicle is small, e.g., thrust accelerations of $10^{-2} g$ or less. This discussion is concerned with the tangentially directed constant thrust program in which the vehicle mass decreases linearly with time. It is assumed that the vehicle commences from a circular satellite and spirals to the point of escape.

The thrust acceleration of this vehicle is given by

$$a = \frac{a_0}{1 - \frac{a_0}{I_{sp} g} t} \quad (\text{B-1})$$

where a_0 is the initial acceleration, I_{sp} is the specific impulse of the propulsion system, and g is the Earth's gravity. The quantity $I_{sp} g/a_0$ has the units of time and is the upper limit of the lifetime of the vehicle.

Consider the growth rate of the osculating semimajor axis s of a low thrust trajectory due to a thrust acceleration applied in the tangential direction. The time derivative of the total orbital energy per unit mass of the vehicle is given by

$$\frac{dE}{dt} = \mathbf{a} \cdot \mathbf{v} \quad (\text{B-2})$$

where \mathbf{v} is its velocity. The quantity E is related to the semimajor axis through the expression

$$E = - \frac{\mu}{2s} \quad (\text{B-3})$$

where μ is GM , the gravitational constant of the planet. From these expressions it follows that the growth rate of the semimajor axis is given by

$$\frac{ds}{dt} = \frac{2s^2}{\mu} \mathbf{a} \cdot \mathbf{v} \quad (\text{B-4})$$

which, for tangential thrust, reduces to

$$\frac{ds}{dt} = \frac{2s^2 a}{\mu} v \quad (\text{B-5})$$

Because of the low thrust, the orbit of the vehicle remains nearly circular (see Fig. 5), and the velocity of the vehicle is nearly the circular velocity

$$v = \sqrt{\frac{\mu}{s}} \quad (\text{B-6})$$

In fact, by an application of a perturbation method to the equations of motion, it may be shown that the actual velocity is related to the instantaneous circular velocity to the first order by the expression

$$v = \sqrt{\frac{\mu}{s}} \left(1 + \frac{a}{\mu/s^2} \sin \theta + \dots \right) \quad (\text{B-7})$$

where θ is the orbital angle. The quantity $a/(\mu/s^2)$ is simply the ratio of thrust to local weight of the vehicle and is, of course, extremely small over all but the last couple of turns of the trajectory. Thus, Eq. (B-6) is a highly accurate approximation over nearly all of the trajectory. Incorporating Eq. (B-1) and this approximation into Eq. (B-2) there results

$$\frac{ds}{dt} = \frac{2s^{\frac{3}{2}} a_0}{\mu^{\frac{1}{2}} \left(1 - \frac{a_0}{I_{sp} g} t \right)} \quad (\text{B-8})$$

which may be integrated. Let us first introduce the dimensionless quantities

$$y = \frac{s}{r_0} \quad (\text{B-9})$$

and

$$\tau = \frac{t}{\frac{1}{a_0}} \sqrt{\frac{\mu}{r_0}} \quad (\text{B-10})$$

where r_0 is the initial satellite radius. The quantity ν is defined as

$$\nu = \frac{1}{I_{sp} g} \sqrt{\frac{\mu}{r_0}} \quad (\text{B-11})$$

Equation (B-8) is now integrated and with these substitutions becomes

$$y = \frac{1}{\left[1 + \frac{1}{\nu} \ln (1 - \nu \tau) \right]^2} \quad (\text{B-12})$$

As $\nu \rightarrow 0$, the thrust acceleration approaches a constant and Eq. (B-12) becomes

$$y = \frac{1}{(1 - \tau)^2} \quad (\nu = 0) \quad (\text{B-13})$$

At escape, y is infinite, and it follows that $\tau = 1$. This implies an escape time of $1/a_0 \sqrt{\mu/r_0}$, which upon comparison with numerical solutions is somewhat high. By the use of Eq. (B-13) in the energy equation

$$E = \frac{1}{2} (\dot{r}^2 + v^2) - \frac{\mu}{r} \quad (\text{B-14})$$

it may be shown that a lower bound for the escape time results. It follows from this that τ is bounded by the inequality

$$1 - \left(\frac{2r_0^2 a_0}{\mu} \right)^{1/4} \leq \tau \leq 1 \quad (\nu = 0) \quad (\text{B-15})$$

For a thrust acceleration of $5 \times 10^{-5}g$ the left-hand side of this expression is 0.9.

An empirical correction factor $\gamma(a_0)$ is introduced which is near the value 1 and is exhibited in Fig. 26.

The escape time for $\nu = 0$ is given by

$$T = \frac{\gamma(a_0)}{a_0} \sqrt{\frac{\mu}{r_0}} \quad (\nu = 0) \quad (\text{B-16})$$

That is, $\gamma(a_0)$ has been designed to give the exact value when $\nu = 0$.

When the l_{sp} is finite, escape occurs at

$$\tau = \frac{1 - e^{-\nu}}{\nu} \quad (\text{B-17})$$

and again employing $\gamma(a_0)$, the escape time is

$$T = \frac{\gamma(a_0)}{a_0} \sqrt{\frac{\mu}{r_0}} \left(\frac{1 - e^{-\nu}}{\nu} \right) \quad (\text{B-18})$$

This expression is remarkably accurate over a wide range of ν . (See Section IV for an illustration.)

In the same manner it is possible to obtain the variation of s with θ , the polar angle. Let

$$x = \frac{\theta}{\Theta} \quad (\text{B-19})$$

where

$$\Theta = \frac{\mu}{4r_0^2 a_0} \quad (\text{B-20})$$

Upon employing the assumption that angular momentum is given by $\sqrt{\mu s}$ it may be shown that

$$\frac{dy}{dx} = \frac{1}{2} y^3 \frac{1}{1 - \nu \tau} \quad (\text{B-21})$$

which may be combined with Eq. (B-12) to yield

$$x = \frac{-4e^{-\nu}}{\nu^4} e^{\frac{\nu}{\sqrt{y}}} \left[\left(\frac{\nu}{\sqrt{y}} \right)^3 - 3 \left(\frac{\nu}{\sqrt{y}} \right)^2 + 6 \left(\frac{\nu}{\sqrt{y}} \right) - 6 \right] + c \quad (\text{B-22})$$

where

$$c = \frac{4}{\nu} \left[1 - \frac{3}{\nu} + \frac{6}{\nu^2} - \frac{6}{\nu^3} \right]$$

At escape

$$x_{\text{escape}} = \frac{4}{\nu} - \frac{12}{\nu^2} + \frac{24}{\nu^3} - \frac{24}{\nu^4} [1 - e^{-\nu}] \quad (\text{B-23})$$

which may be expanded to

$$x = 1 - \frac{\nu}{5} + \frac{\nu^2}{30} - \frac{\nu^3}{210} + \frac{\nu^4}{1680} - \dots \quad (\text{B-24})$$

Equation (B-23) is highly accurate, as may be seen by comparison with Fig. 24, for which escape occurs after 750.434 turns; Eq. (B-23) or (B-24) predict 750.317 turns. Equation (B-22) simplifies, when $\nu = 0$, to

$$y = \frac{1}{\sqrt{1-x}} \quad (\nu = 0) \quad (\text{B-25})$$

and thus Eq. (B-20) yields in radians the number of turns required to escape when $\nu = 0$.

Comparing Eq. (B-13) and (B-25) shows that

$$1 - x = (1 - \tau)^4 \quad (\nu = 0) \quad (\text{B-26})$$

These expressions are also applicable to capture spirals terminating in a circular satellite orbit. In this case, one continues to measure time increasing from the satellite orbit, but ν has a negative value.

For small departures from initial circularity it may be shown that the effect on T and θ at escape involves the eccentricity to only second and higher order powers. By expanding Eq. (B-5) and (B-21) in powers of ϵ_0 and averaging over a period of revolution, it may be shown for an initial orbit of eccentricity ϵ_0 that the time and the number of turns required to escape are given by the approximate expressions

$$T' = T \left(1 - \frac{1}{12} \epsilon_0^2 \right) \quad (\text{B-27})$$

and

$$\theta'_{escape} = \theta_{escape} \left(1 + \frac{1}{6} \epsilon_0^2 \right) \quad (B-28)$$

These expressions do not hold for highly eccentric orbits but are fairly accurate up to eccentricities of 0.5.

For degenerate conic motion with constant thrust acceleration directed along the velocity vector, it may be shown that the escape time from a degenerate ellipse of semimajor axis s_0 is bounded by the inequality

$$1 - \left(\frac{8a_0 s_0^2}{\pi\mu} \right)^{1/4} \leq \frac{T}{\frac{\pi}{2^{3/2}} \cdot \frac{1}{a_0} \sqrt{\frac{\mu}{s_0}}} \leq 1 \quad (B-29)$$

This is similar to Eq. (B-15) and would suggest that the escape time is approximately 10% larger for this extreme case.